CHAPTER 5

DEVELOPMENT, CHARACTERIZATION AND EVALUATION OF NANOVESICLES FOR NOSE TO BRAIN DELIVERY OF OXYTOCIN AND VASOPRESSIN

"Learning gives creativity, creativity leads to thinking, thinking provides knowledge, and knowledge makes you great."

- A.P.J. Abdul Kalam

Development, characterization and evaluation of liposomes for nose to brain delivery of oxytocin and vasopressin

5.1 Background

Due to unfavourable drug conditions and the brain's selective barrier provides low absorption and therapeutic delivery. This remains the largest obstacle in clinical development [1]. The complex anatomical and physiology of BBB prevents active molecules to enter from brain or CNS that makes brain delivery a herculean task [1]. 98% of new molecules meant for CNS are being devoided of entry to brain due to their physicochemical and biological characteristics. Within the CNS and circulating blood vessels, interstitial fluid serves as main barrier [2]. Additionally, the BBB contains a number of transporter systems that directly prevent drug molecules from entering brain. The P-glycoprotein (PgP) efflux transporter is the most prominent example.

This restricts the therapeutic concentration and distribution of drugs to brain. Thus, reduces their effectiveness and prolongs the course of treatment for a number of conditions associated with CNS, including meningitis, Parkinson's, schizophrenia, Alzheimer's, brain tumours, and migraine [3]. Numerous researchers have developed several kinds of methodologies and alternate pathways. It includes invasive and non-invasive techniques, to achieve therapeutic concentrations in CNS.

In recent times, scientists have placed greater emphasis on creating non-invasive methods to deliver therapeutic substances straight to CNS. This interest is particularly directed toward leveraging the unique pathways of trigeminal and olfactory systems, which offer potential solutions for overcoming the significant challenges presented by BBB. Over the past two decades, this innovative approach to brain delivery via nasal route has garnered profound attention as a promising avenue for effective treatment strategies [3]. Benefits of nasal delivery to the brain include safety, effectiveness, non-invasiveness, lack of hepatic metabolism, ease of administration, and, most importantly, the ability to be self-administered. Drug molecules can enter the brain directly to certain regions of nose. The olfactory and trigeminal parts of nasal anatomy are a few such regions. The olfactory region, which plays a crucial role in our sense of smell, is equipped with specialized olfactory receptors and olfactory neurons. These neurons have axon extensions that project into the olfactory bulb, allowing this region to establish direct access to the central nervous system.

The olfactory region is uniquely identified as only peripheral part of body that maintains a direct connection to brain, making it a fascinating area of study. Numerous pre-clinical and clinical research efforts highlighted nose to brain pathway presents a promising non-invasive approach for drug delivery, potentially circumventing the formidable BBB that typically restricts medication access to CNS. However, despite these noteworthy advantages, it has been observed that a mere 0.1% of the drug administered can successfully penetrate CNS through this nasal-to-brain route. When a formulation is administered via nasal route, it directly traverses into CNS. Thereby, bypassing the protective barrier that usually guards against foreign substances. Nonetheless, the process is not without its challenges. The major factors include enzymatic breakdown that occurs in nasal cavity, mucociliary clearance mechanisms, and limitations on dose volume typically restricted to between 25 and 200 µL pose significant hurdles for efficacy of nose-to-brain delivery. Despite these limitations, this method still offers the distinct advantage of potentially reducing overall dosage needed for therapeutic effect.
The intricate challenge of effectively delivering medications from nasal cavity directly to brain has posed significant obstacles, greatly hampering commercial advancement of this promising and innovative therapeutic route [2, 4]. To address this limitation, researchers are pursuing with innovative strategies aimed at improving the feasibility of this delivery method. They are concentrating on developing advanced drug delivery systems and exploring innovative nanotechnology-driven solutions to address current challenges and realize the complete potential of this method.

In this work, design, development and characterisation of peptide loaded in lipids were prepared using simple precipitation method followed by size reduction technique. In this combination of HSPC and MPEG (2000)-DSPE was used, and cholesterol incorporated as membrane fluidity homeostasis. The formulated liposomes were meant for pharmacological evaluation using In vitro and preclinical AD model. Further preclinical pharmacodynamic evaluation was done for Intranasal and Intravenous route. The proposed hypothesis is unique and novel in terms of dosage form, strategy for administration and compositions of delivery systems, which enhances patentability as well as commercialization aspects.

5.2 Materials and Instruments

The materials utilized in this research are shown in Table 5.1. The information regarding the instruments employed is presented in Table 5.2.

Table 5.1: List of raw materials and chemicals used in current research work

Material	Source
Antibiotic solution	Sigma, Mumbai, India
4',6-Diamidino-2-Phenylindole, Dihydrochloride (DAPI)	Sigma, Mumbai, India
Acetonitrile (LiChrosolv®) for chromatography	Merck, Mumbai, India
Acetonitrile for HPLC	Spectrochem, Mumbai, India
Anti-Bim polyclonal antibody (PA5-20089)	Pierce/Thermo Scientific, USA
cDNA synthesis kit	HiMedia, Mumbai, India
Cholesterol	Phospholipid GMbH, Germany
Coumarin-6	Fluka Biochemica, Sigma-Aldrich Inc., MO, USA
Culture plate (6, 24 and 96 well)	Costars, Corning Inc., NY, USA
Custom-designed PCR array plates	Life Technologies, USA
Cytokine's detection kits	eBioscience, USA
Dialysis membrane with MWCO-12 kDa	Himedia, Mumbai, India
Dimethyl formamide (DMF)	Central Drug House, New Delhi, India
Dimethyl sulphoxide (DMSO)	Merck, Mumbai, India
Distilled water	Scientronic, Germany
DMSO	Merck Specialities Pvt. Ltd., Mumbai, India
Dulbecco's Modified Eagle's Medium-high glucose	Merck, Mumbai, India
ECL reagents	Pierce, USA
Ethanol, absolute	Hong Yang Chemical Corporation, China
Fetal Bovine Serum (FBS)	Merck Specialities Pvt. Ltd., Mumbai, India
Hydrochloric acid	J T Baker, USA
Isopropyl alcohol	LobaChemie, Mumbai, India
Lipopolysaccharide (LPS)	Sigma, USA
Methanol HPLC grade	Merck India Ltd., Mumbai, India
Microbial Culture SH-SY	American Type Culture Collection (ATCC), Mannasse, Virginia, USA
Microscopic cover glass	Blue Star®, Polar industrial, Mumbai, India
Microtiter plates (96 well)	B.D. Biosciences, USA
Monosodium hydrogen phosphate	Merck, USA
MPEG (2000)-DSPE	Phospholipid GMbH, Germany
MTT (3-(4, 5-dimethylthiazolyl-2)-2, 5-diphenyltetrazolium bromide)	Sigma-Aldrich, St. Louis, USA)
Needles (Hypodermic-BD)	Beckton Dickinson and Co., USA
Oxytocin	Sun Pharmaceutical Industries Ltd, Ahmednagar, India
Paraformaldehyde	Merck, India
Peroxidase-conjugated secondary antibodies (NFkB)	Cell Signaling and Abcam

Material	Source
Phosphotungstic acid	S.D. Fine, Mumbai, India
Pierce ECL Western blotting substrate	Pierce Scientific, USA
Phorbol-12-myristate-13-acetate (PMA)	Wako, Japan
Polycarbonate membrane filters (0.025, 0.05, 0.1 & 0.2 µm)	Whatman Inc., New Jersey, USA
Potassium bromide	SRL, Mumbai, India
Propidium iodide (PI) staining kit	eBioscience, USA
SH-SY5Y	NCCS, Pune, India.
Sodium chloride	Merck, India
Sodium citrate	Merck, India
Cytokines and Apoptotic markers	Cell Signaling and Abcam
Triton X 100	Merck, USA
Tween 20	Merck, USA
Water for Injection	Mili-Q
Water, for HPLC	Merck Specialties Private Limited, Mumbai, India
Whatman filters	Instruchemie, Delfzijl, the Netherlands
Trizol reagent	Sigma Aldrich, MA, USA
cDNA synthesis kit	HiMedia, Mumbai, India

Table 5.2: Details of various instruments employed during the current research work

Equipment	Model Number	Manufacturer
Bath sonicator	Branson Ultrasonic cleaner 3210E-DTH TOSHCON-400KUS20	Branson Ultrasonics Corporation, Connecticut, USA
Centrifuge	Bench Model Remi R-24	Sartorious, Germany Remi Motors, Mumbai, India
Fluorescence microscopy		NIKON-Ti2, US
Cyclomixer	CM101	Remi Motors, Mumbai, India
Camera	Nikon Model: S50	Nikon, Japan
Deep Freezer (-20ºC)	Vertical Deep Freezer FS-345 (345 L)	Blue Star, Mumbai, India
Deep Freezer (-80ºC)	V-410 Ultra low freezer	New Burnswick Scientific, France
Differential scanning calorimeter	DSC 821 DSC-Q20	Mettler Toledo, Switzerland TA Instruments, USA
Freeze Dryer	SNL216V-230 Alpha 2-4 LD Plus	Thermo Electron (Thermo Sawant), USA Martin Christ GmbH, Germany Vir Tis, Wizard 2.0, New York, USA
Fourier Transform Infrared spectroscopy (FTIR)	RX-100	Perkin Elmer, U.S.A.
Haemocytometer	Neubauer	Fein-Optik, Germany
High performance liquid chromatography (HPLC)	2010CHT	Shimadzu, Japan
HPLC column	CAPCELL PAK C18 MG II, 4.6 mm I.D. X 250 mm	M/s Waters Corporation, Milford, USA

Equipment	Model Number	Manufacturer
Magnetic stirrer (Thermostatic)	1MLH, 2MLH Spinot™	Remi Motors, Mumbai, India Tarsons Products, Calcutta, India
Mechanical Stirrer	RQ 122	Remi Motors, Mumbai, India
Mega View II digital camera	H-7000	Hitachi, Japan
Microscope, attached with a camera and fluorescence filters	TE 2000-S, camera DS-5M-L1	Nikon Corporation, Japan
Microscope	TELAVAL 31 Nikon eclipse 80i	Carl Zeiss, Germany Nikon Corporation, Japan
Membrane filtration assembly	25 mm, 47 mm	Millipore, USA
Particle Size Analyzer	Mastersizer-2000, Zetasizer 2000HS	Malvern Instruments Limited, UK
	Malvern Zetasizer, Nano ZS 90	Malvern Instruments Limited, UK
Phase contrast microscope	Kyowo-Getner	Medilux, Japan
pH meter	Mettler Toledo	Mettler Toledo
Pipettes	71050XET, 720020 and 720070	BIOHIT OYJ, Finland
Reverse Osmosis (RO) water system	Milipore Direct®	Millipore India Pvt. Ltd., Bangalore, India
Rotary evaporator	Laborota 4011/HB/G3	Heidolph Instruments GmbH, Germany
Stage Micrometer	Fein-Optik, Germany	Fein-Optik, Germany
Transmission electron microscope	H-7000	Hitachi Ltd., Japan
Vacuum pump	-	Welch Rietschle Thomas Skokie, USA
Vortex mixer	CM101	Remi Motors, Mumbai, India
Weighing balance (electronic)	AE240, BB244	Mettler Analytical Balances, Switzerland
qRT-PCR	Step One Plus Real-Time PCR system	Applied Biosystem
iScript cDNA kit		Biorad, USA
Multimode reader		Agilent, Biotek, US

5.3 Preparation, characterization and evaluation of drug loaded liposomes

5.3.1 Fabrication of Liposomes for Oxytocin and Vasopressin

The lipids of HSPC, MPEG (2000)-DSPE, and cholesterol, were mixed in 15 mL of absolute ethanol. To this solution, Oxytocin/vasopressin was added respectively at a temperature of 40 °C for 15 minutes. This lipid mixture was subsequently injected into an acetate buffer saline (pH 4.0) while stirring continuously at 250 rpm. The solution was stirred for an additional 30-

45 minutes. The resulting liposomes were processed through a series of size-extrusion steps using 0.40/0.20 µm and 0.20 µm Whatman filters to achieve a uniform particle size (PS) [5].

5.3.2 Methodology for characterization of liposomes

5.3.2.1 Micromeritics of liposomes

The Malvern Nano-ZS (Zeta sizer) was employed to analyse various characteristics of samples, including Zeta potential (ζ, ZP), particle size (PS), and polydispersity index (PDI). To gain insights into the average dimensions of vesicles, as well as their PDI and surface charge (ZP), photon correlation spectroscopy was utilized.

In order to carry out measurements, the sample was carefully placed into a cuvette designed for this purpose. The dynamic light scattering (DLS) method was then applied to accurately measure particle size of vesicles that had been prepared. This technique takes advantage of the natural movement of particles under Brownian motion, allowing DLS to assess their diffusion rates. The Stokes-Einstein relationship is subsequently employed to convert these diffusion measurements into precise size and distribution data.

ZP studies provide basis for stability of liposomes [6]. The ZP of formulated liposomes was evaluated using laser Doppler anemometry with folded capillary cells. ZP of well-dispersed liposomes in a deionized water sample was measured at 25 ± 0.1°C and an electric field strength of 15.24 V/cm. All samples were analysed in triplicate [3].

In addition, detailed surface structure of the finished liposomes was meticulously examined using High Resolution Transmission Electron Microscopy (HR-TEM). To facilitate this analysis, a small volume (approximately 10 µL) of the liposomal suspension was carefully deposited onto carbon-coated microscopic grids, allowing the particles to adsorb onto surface. Following this, the grids underwent a treatment with a 1% (w/v) aqueous solution of phosphotungstic acid, a step essential for negative staining, to enhance contrast. Once dried, the grids were scrutinized under HR-TEM at appropriate magnifications, with the microscope operating at a precise acceleration voltage of 200 kV to capture clear and detailed images [7].

5.3.2.2 Percentage drug entrapment (%EE)

%EE was assessed using the direct lysis method [8]. In summary, the EE of liposomes were measured in three separate trials. The liposomal suspension containing oxytocin and

vasopressin was centrifuged at 25000 rpm at 5°C for 30 minutes to isolate pellet of liposomes from supernatant. Clear supernatants as well as vesicular sedimented pellet were collected separately. Sediments were individually lysed with methanol mixture and samples were collected. The appropriate dilutions of samples were made and analysed to quantify Oxytocin and Vasopressin by validated HPLC method. %EE of drug was calculated using following equation 5.1:

$$\%EE = \frac{(T-C)}{T} X\ 100 \ldots\ldots\ldots \text{eq. 5.1.}$$

Whereas, C represents the quantity of oxytocin/vasopressin found in the supernatant, T signifies the overall amount of oxytocin/vasopressin identified in both sediment and supernatant.

5.3.3 Optimization of liposomes for Oxytocin

In order to get a final liposome with desired size (<100 nm), narrow PDI (<0.5), high entrapment efficiency, and maximum drug loading, a number of formulation and process factors were optimized for development of liposomes while maintaining a constant drug amount. During preparation of liposomes the operational temperature was kept ~ 40°C to safeguard the peptide molecules from higher temperature.

5.3.3.1 Optimization of lipid ratio

Liposomes formulation were prepared by varying the ratio (w/w/w) of HSPC, MPEG (2000)-DSPE and cholesterol while keeping amount of HSPC constant and other process parameters were kept constant (stirring speed- 300 rpm, stirring time-45 minutes). Optimization was done on basis of average PS, PDI and %EE of liposomes (Lipo). PS and PDI was determined by using Malvern Zetasizer, while, %EE was done by direct HPLC method [9]. The molar ratio from 4:0.5:0.5 to 4:1:1.5 was optimised for HSPC: MPEG (2000)-DSPE: Cholesterol.

5.3.3.2 Optimization of process variables

5.3.3.2.1 Stirring speed

The speed of stirring was varied ranging from 100 to 400 rpm for liposomes preparation using the same optimized formulation parameters. The PS and %EE of prepared liposomes were determined for further optimization [9].

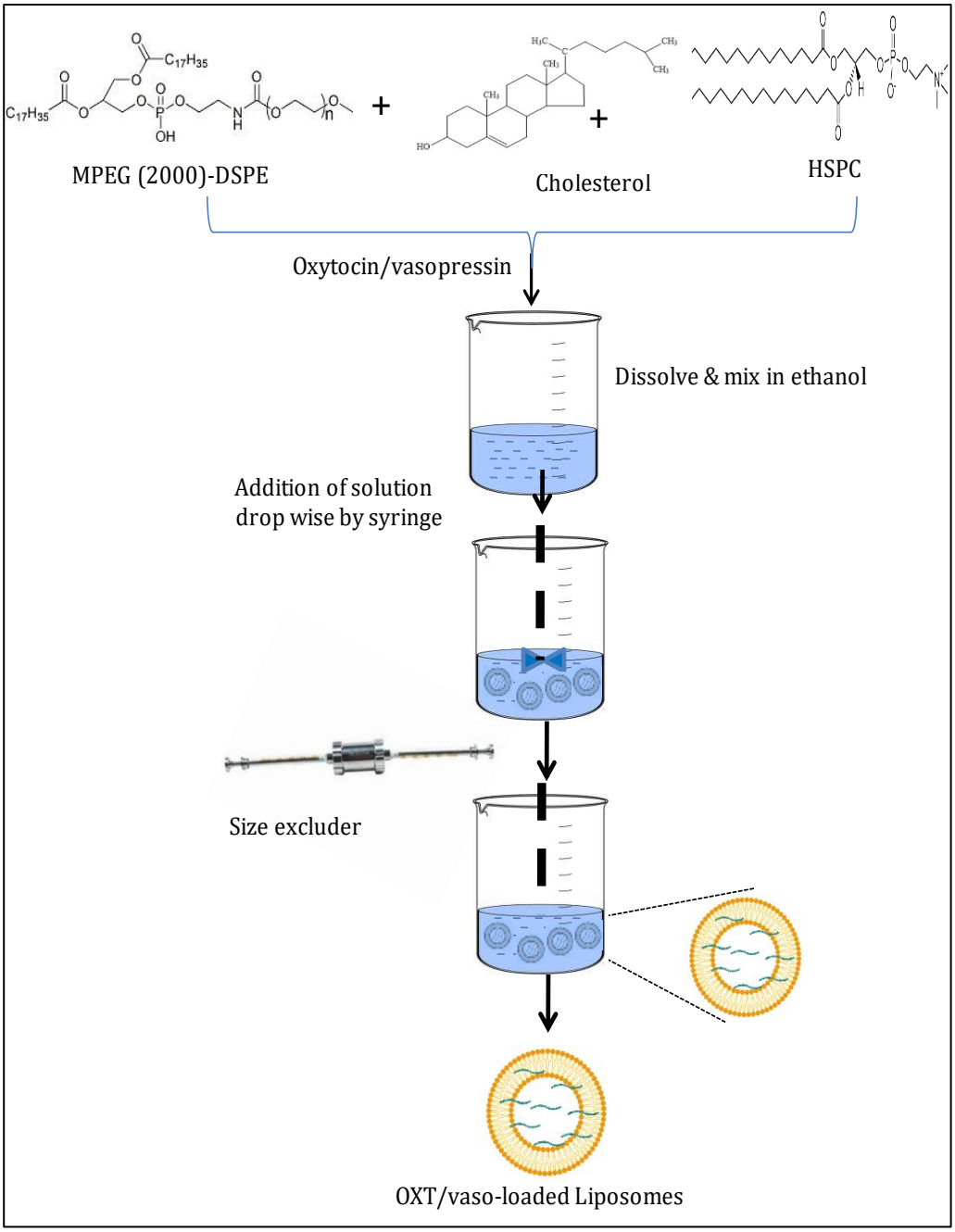

Figure 5. 1: Schematic presentation of fabrication of liposomes

5.3.3.2.2 Stirring time

For the optimization of stirring time, formulation F8 was selected while remaining process variables were kept fixed. The liposomes dispersions were prepared with different stirring time (*viz.* 30, 45, 60 min.). PS and %EE were determined for selection of optimized parameters [9].

5.3.4 Optimization of liposomes for vasopressin

Vasopressin and Oxytocin are two closely related neuropeptides, both comprising of nine amino acids differing at 3rd and 8th position respectively. Both the peptides have molecular weight in approximately similar range [9]. Therefore, similar optimization strategy was evaluated for the development of liposomes of vasopressin.

5.3.4.1 Optimization of lipids ratio

Liposomes formulation for Vasopressin were prepared by varying the ratio (w/w/w) of HSPC, MPEG (2000)-DSPE and cholesterol while keeping the amount of HSPC constant and other parameters were kept constant (stirring speed- 300 rpm, stirring time-45 min). Optimization was done on the basis of average PS and PDI of liposomes which was determined by using Malvern Zetasizer [9].

5.3.4.2 Optimization of process variables

5.3.4.2.1 Stirring speed

Procedure as mentioned in section 5.3.3.2.1.

5.3.4.2.2 Stirring time

For the optimization of stirring time, formulation F8 was selected while remaining process variables were kept fixed. Procedure as mentioned in section 5.3.3.2.2.

5.3.5 Stability of liposomes formulations

The stability of liposomal dispersions loaded with drugs (Oxytocin and Vasopressin) was investigated at temperatures of 2-8°C and 25±2°C with 60±5% RH for 3 and 6 months, respectively [9]. Throughout this timeframe, samples were systematically collected at designated intervals for thorough analysis, which included evaluating the percentage assay, measuring PS, assessing ZP, determining PDI.,

5.3.6 *In vitro* cell line study

5.3.6.1 % Cell viability and Cell uptake study on SH-SY5Y cells

5.3.6.1.1 Cell culture

SH-SY5Y cells were cultured in T-25 flasks using a culture medium of DMEM, which was enhanced with 1% antibiotic solution (Streptomycin/penicillin) to prevent contamination, and 10% Fetal Bovine Serum to provide essential nutrients for cell growth. To ensure optimal humidity levels for the cells, a saturated copper sulphate solution was employed throughout their 24-hour incubation period in a controlled environment, where the carbon dioxide concentration was meticulously maintained at 37°C ± 0.5%. Once the incubation period ended, old media was carefully taken out, and cells were gently rinsed with phosphate-buffered saline (PBS) at a pH of 7.4. After this washing step, new media with 10% FBS and 1% antibiotic was thoughtfully added to revitalize the cell cultures [10].

5.3.6.1.2 % of Cell viability and biocompatibility

The percentage of cell viability was assessed using MTT method, following previously published literature [9, 10]. This test was employed to evaluate biocompatibility of liposome formulations in neuro cells. In a series of 96-well microtiter plates, SH-SY5Y cells were carefully seeded, and SH-SY5Y cells, with a density of $5x10^3$, were plated in a 96-well plate and treated with varying concentrations (1, 10, 100 µg/mL) of oxytocin, vasopressin, OXT-loaded liposomes, Vaso-loaded liposomes, plain liposomes (Placebo), and phosphate buffer saline (PBS)-treated cells served as controls. The treatments were administered over three distinct time periods: 24, 48, and 72 hours. After completing each treatment duration, 20 µL of MTT dye solution, prepared at a concentration of 5 mg/mL, was carefully added to each well. Following the addition of dye, wells were thoroughly rinsed with PBS adjusted to a pH of 7.4 to ensure accurate results. To dissolve the formazan crystals, 100 µL of DMSO was added after an incubation of 4 hours. The intensity of dissolved formazan was measured using a BIORAD microplate reader at a wavelength of 570 nm. The absorbance of treated wells was compared to that of PBS-treated cells and considered as 100% viable. PBS 7.4 and Triton X 100 served as positive and negative controls, respectively [10].

5.3.6.1.3 Cell permeation study (Cell uptake)

Qualitatively cell uptake study was performed as method is mentioned in published reports [9-11]. SH-SY5Y cells with $1x10^5$ population were used to assess intracellular localization of coumarin-6 (C-6) and C-6-loaded liposomes (Lipo) formulations. First, C-6 & oxytocin co-encapsulated Lipo, and C-6 & vasopressin co-encapsulated Lipo were formulated for cell uptake study in SH-SY5Y. C-6 was dissolved in ethanol along with drug. The remaining procedure was same as mentioned for liposomes formulation in section 5.3.1.

A 6-well plate was meticulously arranged, with each well containing $1x10^5$ SH-SY5Y neuroblastoma cells, and incubated in an incubator with 5% CO_2 at 37ºC temperature for overnight to allow cells to firmly adhere with plate surface. The following day, adherent cells were carefully treated with C-6, C-6 + OXT, C-6+Vaso, C-6-OXT-Lipo and C-6-Vaso-Lipo, at a concentration of 4 µg/mL, which is equivalent to C-6, for a duration of 4 hours at a controlled temperature of 37ºC. After the treatment period, thorough washing of cells, receiving five washes with 1X HBSS to effectively remove any excess fluorescent dye and uninternalized Lipo. To preserve the cellular structure for imaging, cells were then fixed with a 4% paraformaldehyde solution and subsequently examined under a fluorescence microscopy (NIKON-Ti2, US) using a green filter.

5.3.6.1.4 Cell apoptosis assay

Acridine orange (AO) and ethidium bromide (EB) dyes are highly effective tools employed to illuminate any nuclear alterations and formation of apoptotic bodies. The both of them serve as vital indicators of apoptosis within cells. AO, a cationic dye, possesses unique ability to easily penetrate intact membranes of both viable and non-viable cells. The results in a radiant green fluorescence that serves to vividly highlight living cells amidst their environment. In contrast, EB infiltrates damaged membrane cells. The cellular integrity is frequently associated with onset of apoptosis emitting a striking red fluorescence marks the presence of dead cells within sample.

For experimentation 12-well plate was utilized, with SH-SY5Y cells carefully seeded at a density of 1×10^5 cells per well, ensuring uniform distribution. Following this seeding process, the cells were subjected to a 24-hour incubation period. This allows ample time for them to adhere firmly to well surface and grow. After this incubation phase, the cells were treated with

a substantial concentration of 100 µg/mL of oxytocin and vasopressin, in conjunction with their encapsulated Lipo, to effectively induce apoptosis and observe corresponding cellular responses.

After an additional 48 hours of incubation, the cells were washed three times with sterile PBS at pH 7.4 to remove any excess substances. Subsequently, 0.2 mM of AO and 1 mM of EB were incubated to each well, enabling a qualitative assessment of degree of apoptosis in treated cells. Finally, images were captured using a fluorescent microscope set at a 20 X magnification, allowing for detailed visualization of any apoptotic changes.

5.3.6.1.5 Reactive Oxygen Species (ROS) Assay

ROS are highly reactive molecules characterized by one or more unpaired electrons, which are generated during the reduction of molecular oxygen. When ROS are produced in excess, they can cause significant oxidative damage to cellular components, including proteins, DNA, and lipids, particularly under influence of potent chemotherapeutic agents. This overproduction of ROS can trigger a cascade of detrimental effects, leading to disrupted cellular functions, impaired redox regulation, programmed cell death (apoptosis), and ultimately cell death.

To investigate and qualitatively assess the generation of ROS within cells, researchers employ a cationic lipophilic green fluorescent dye known as DCFDA (2',7'-dichlorodihydrofluorescein diacetate). Once inside the cells, cellular esterases act on DCFDA, hydrolysing it to form DCF, which is fluorescent. This transformed compound then reacts with ROS and results in green fluorescence that can be visualized under a microscope. In this specific experiment, SH-SY5Y neuroblastoma cells were plated in 12-well plate at a concentration of 1×10^5 cells per well and incubated for 24 hours to guarantee adequate attachment and growth. Following this incubation period, the cells were subjected to treatment with high concentrations (100 µg/mL) of oxytocin, vasopressin, as well as specialized liposomes containing either oxytocin or vasopressin. After an additional 48 hours of treatment, the cells were carefully rinsed three times with PBS at a physiological pH of 7.4 to remove any unbound compounds.

Subsequently, each well was incubated for 30 minutes with 1 µL of DCFDA solution (at a concentration of 1 mg/mL), diluted in PBS. This incubation allowed for the effective uptake of the dye and its reaction with any ROS present inside the cells. Following the treatment, cells were examined under a fluorescent microscope set to a magnification of 20X, utilizing a green

filter to clearly visualize the fluorescence emitted by the DCF, indicating the presence and activity of ROS within the cells.

5.3.6.2 Evaluation on monocytic cells (THP-I)

5.3.6.2.1 Genomic microarray (qRT-PCR) analysis

Human THP-I cells were carefully prepared by seeding them at a density of 4×10^4 cells per well in 96-well plates. These cells were cultured for a period of 24 hours to allow for optimal growth and adherence. After the initial incubation period, 100 nM phorbol 12-myristate 13-acetate (PMA) was carefully administered to wells, providing a potent stimulus for cells. These cells were then maintained in this supportive and activating environment for an extended duration of 24 hours, facilitating their transformation into fully differentiated mature macrophages.

After the differentiation period, hTHP-1 cells were thoroughly washed with fresh culture media to eliminate any remaining PMA and were then placed in a resting state for an additional 24 hours. Once adequately rested, the cells underwent stimulation with 1 µg/mL of ultrapure lipopolysaccharide (LPS) for a 24-hour duration, initiating an inflammatory response.

In the next phase, cells were treated with various drug solutions and drug-loaded liposomes, allowing for a precise 2-hour incubation period to facilitate interaction. After this incubation, the media were carefully removed, and to facilitate cell detachment, 1 mL of 0.5M EDTA was introduced. The cells were then incubated for 15 minutes to ensure effective detachment.

Initially, the cells were carefully subjected to centrifugation at a speed of 1,700 rpm for a precise duration of 10 minutes to separate cellular components. Once the centrifugation process was complete, resulting supernatant was discarded, and cells underwent two washes with PBS to effectively eliminate any remaining contaminants.

For RNA extraction, total RNA was obtained from both LPS-treated and untreated THP-1 cells using RNeasy Mini Kit, recognized for its reliability in isolating high-quality RNA. Following extraction, the quantity of RNA was accurately measured to ensure sufficient amounts for further analysis. The isolated RNA was then reverse transcribed into complementary DNA (cDNA) employing the iScript cDNA kit, setting the stage for upcoming quantitative reverse transcription polymerase chain reaction (qRT-PCR) analysis.

Detailed information about the specific primer sequences and functional roles of all analysed genes is provided in Table 5.3. The expression levels of mRNA were quantified utilizing ΔΔCT method and subsequently normalized against housekeeping gene ACTB, which encodes for β-actin. This guaranteed precise and meaningful comparisons across the data set.

Table 5. 3: The information of primer sequences for all genes

S. No	Gene	Role of gene	Forward (5'-3')	Reverse (5'-3')
I	CAS3	Apoptotic	CATGGAAGCGAATCAATGGACT	CTGTACCAGACCGAGATGTCA
II	CD40	Apoptotic	CAGCCAGGACAGAAACTGGTGAGT	CTTCTTCACAGGTGCAGATGGTGTC
III	BIM	Pro-apoptotic	GGCCCCTACCTCCCTACA	GGGGTTTGTGTTGATTTGTCA
IV	BAK	Pro-apoptotic	TTTTCCGCAGCTACGTTTTT	GGTGGCAATCTTGGTGAAGT
V	IL-6	Inflammatory	AGCCACTCACCTCTTCAGAAC	GCCTCTTTGCTGCTTTCACAC
VI	CAS8	Apoptotic	TGGTCTGAAGGCTGGTTGTT	AAGTGACCAACTCAAGGGCT
VII	CAS9	Apoptotic	GGACATGCTGGCTTCGTTTC	GGTCTTTCTGCTCGACATC
VIII	AKT	Apoptotic	TCTATGGCGCTGAGATTGTG	CTTAATGTGCCCGTCCTTGT
IX	NFKβ	Inflammatory	TGAGTCCTGCTCCTTCCA	GCTTCGGTGTAGCCCATT
X	BCL	Anti-apoptotic	GTAAACTGGGGTCGCATTGT	TGGATCCAAGGCTCTAGGTG

5.3.6.2.2 Immunofluorescence assay (IFA)

THP-1 cells underwent differentiation process into macrophage-like cells and studied for range of treatments, like OXT, Vasopressin, OXT-Lipo, and Vaso-Lipo. Following a 24-hour incubation period that allowed cells to absorb the treatments. The cells were then thoroughly rinsed with PBS, ensuring the complete removal of any remaining residual substances that could interfere. The washed cells were fixed with a 4% paraformaldehyde solution for 5 to 10 minutes. A step crucial for preserving cellular structure, after which they were permeabilized for 3 minutes using a 0.1% Triton X-100 solution, facilitating antibody access to intracellular components.

The fixed and permeabilized cells were then subjected to a blocking step. They were incubated in a 5% bovine serum albumin (BSA) solution in PBS for 1 hour to minimize non-specific binding. Following this, the cells were treated with a primary antibody targeting FOXO, diluted

at a ratio of 1:200, for a duration of 2 hours to ensure optimal binding. After an appropriate washing step to remove unbound antibodies, the hTHP-1 cells were treated with a fluorescently labelled FITC-conjugated anti-rabbit IgG antibody for one hour, allowing for visualization of the FOXO protein.

The antibody-stained cells were then meticulously placed onto glass cover slips, washed again to eliminate any excess reagent, and mounted using an anti-fade medium containing DAPI, which stains nuclei. Finally, high-resolution images of the stained cells were captured using a confocal microscope, providing detailed insights into the cellular localization and expression of FOXO [11-14].

5.3.7 Neurological activities of developed formulations in experimental animals

5.3.7.1 Rationale for *In vivo* studies

In the realm of neuro-pharmacological research, researchers confront a unique array of challenges due to an intricate and multifaceted nature of these conditions. Neurological disorders are not merely isolated issues. They involve a complex interplay of various patho-physiological processes that interact dynamically, making them difficult to replicate accurately within the confines of a controlled laboratory environment. The limitations of conventional models mean that critical aspects of brain function, behaviour, and the intricate ways in these disorders manifest may be overlooked, hindering the development of effective treatments and therapies. Thus, advancing our understanding of these complex diseases requires innovative approaches that go beyond standard laboratory techniques.

Given these challenges, it becomes imperative to explore the effectiveness of Oxytocin-loaded and Vasopressin-loaded liposomes as delivery systems for therapeutics intended for the brain. This investigation should not only focus on their ability to transport these compounds across BBB but also examine the resulting impacts on disease symptoms and underlying pathology. Such studies should be conducted using relevant animal models that accurately represent various neurological and neuropsychiatric conditions. Preclinical requisites are as follows. Male Balb/C mice, aged 8 to 10 weeks and weighing between 25 and 40 grams, were chosen as the subjects for in vivo testing. The mice were housed in groups of six under controlled humidity and temperature conditions. They had continuous access to Laboratory Rodent Diet food and water, following a protocol approved by the institutional committee. The lights in the

mouse housing rooms were turned off every evening at 6 p.m. and turned back on at 6 a.m. to maintain a 12-hour light/dark cycle.

All experimental treatments, research on gene expression, studies involving the hippocampus, and evaluations of cognitive function were conducted. Cognitive function assessments included performance in the Morris Water Maze (MWM) for learning and memory tasks i.e., cognitive studies. Further studies include biochemical, gene expression and histopathological studies. The National Institute of Occupational Health (NIOH), Ahmedabad's Institutional Animal Ethical Committee reviewed and approved the methods used to treat all of the study's animals (NO: *IAEC-ICMR-NIOH/2022-23/29/02/M*).

5.3.7.2 Morris water maze test (MWM)

Liposomes containing drugs were administered through intranasal (IN) and intravenous (IV) methods, and their effects were compared to those of a free drug solution also given via these routes, using the MWM test [17–21]. Mice underwent four days of training to learn how to reach the hidden platform located in the fourth quadrant. After this training period, a final acquisition trial was performed after the treatment. Further information regarding the groups and treatments is provided below.

Because their initial group weights were similar, mice were randomized according to their weights and grouped for treatment.

(i) control or untreated mice;

(ii) mice that received Scopolamine (SCP) intraperitoneal (IP) or positive control (n = 6); and mice that undergone different types of therapy or intervention groups following SCP (2 mg/kg), IP. Injection viz.;

(iii) Vasopressin drug solution (2 µg dose per animal) IN (n = 6),

(iv) Vasopressin loaded Lipo (equ. 2 µg Vaso per animal) IN (n = 6),

(v) Vasopressin loaded Lipo (equ. 2 µg Vaso per animal) IV (n = 6),

(vi) Vasopressin drug solution (2 µg Vaso per animal) IV (n =6),

(vii) Oxytocin drug solution (equivalent to 100 µg oxytocin) IN (n = 6),

(viii) Oxytocin loaded Lipo (equivalent to 100 µg oxytocin) IN (n = 6),

(ix) Oxytocin loaded Lipo (equivalent to 100 µg oxytocin) IV (n =6),

(x) Oxytocin drug solution (equivalent to 100 µg oxytocin) IV (n = 6)

In the MWM test, factors monitored included: the duration taken to locate the hidden platform and amount of time mice spent in fourth quadrant [19]. SCP and naïve treated group were control for comparison. The heat map and graphs were studied to find hidden platform in fourth quadrant.

5.3.7.3 Brain Hippocampus histopathological evaluation

The study conducted a thorough evaluation of effectiveness of proposed formulations by examining histological characteristics of hippocampal tissue. A key indicator of successful treatment is a higher density of neurons, which correlates with improved outcomes. As outlined in the methodology, the experimental process involved euthanizing the mice at the end of treatment regimen, allowing for acquisition of brain tissue. Once removed, the brains were carefully immersed in a fresh solution of formaldehyde for a duration of 24 hours to preserve tissue and prevent degradation. Following the fixation process, a meticulous dehydration procedure was initiated. This involved sequentially immersing the brain tissue in ethanol at varying concentrations: first in a 70% ethanol solution for 24 hours, then shifting to 90% ethanol for 1 hour, and finally immersing in 100% ethanol for another hour. This step ensured the removal of water from the tissue, making it suitable for embedding. After the dehydration process, the brains underwent a clearing stage using xylene, which aids in the removal of ethanol and prepares the tissue for embedding in paraffin. The embedding was performed to create a solid block that facilitates sectioning.

Using a microtome, coronal sections of precisely 5 µm in thickness were cut from the paraffin-embedded brain tissue. These thin slices were then carefully placed onto glass slides. To enhance the visibility of cellular structures, the sections were stained utilizing the standard hematoxylin and eosin staining technique, which is widely recognized in histology for highlighting different tissue components [17-24]. This comprehensive approach allowed for an in-depth analysis of the neuronal density and overall health of the hippocampal tissue, leading to a robust assessment of formulations' effectiveness.

5.3.7.4 Gene Expression Studies

To establish the molecular effectiveness of aforementioned treatment, conducting gene expression studies is essential. These studies were focused on analysing brain homogenate samples, which provided deep insights into the expression levels of key biomarkers. Specifically, the investigation examined the following factors: AIF-1 (Allograft inflammatory factor 1), known for its role in inflammation; BDNF (brain-derived neurotrophic factor), a critical protein involved in the survival and growth of neurons; GFAP (glial fibrillary acidic protein), a marker of astrocytic activation; IL-6 (interleukin-6), an important cytokine involved in inflammatory responses; and Nrf 2 (nuclear related factor 2), a vital regulator of antioxidant response. These analyses are instrumental in understanding the underlying molecular mechanisms and potential therapeutic effects of the treatment [19,20, 24].

The sagittal entire section of each mouse's brain was used for gene expression analysis. Total RNA from collected brain tissues was extracted using the Trizol reagent. At initial stage, quality and purity assessment of extracted RNA was conducted in order to ensure proper downstream processing. 1000 ng of total RNA was transformed into a cDNA for amplification employing a cDNA synthesis kit. These tissues were subjected to qRT-PCR-based relative gene expressions for a variety of genes using SYBR green dye and proper primers (Table 5.4). 40 cycles of 95 and 60°C for one minute each condition was followed using qRT-PCR. Data were analysed using the $2^{-\Delta\Delta Ct}$ method and values are expressed as fold change relative to the control group [19,20].

Table 5.4: Primers of Genes for qRT-PCR with their role in brain

Gene	Role	Forward (5′−3′)	Reverse (5′−3′)
AIF-1 (Allograft inflammatory factor 1)	prominent neurodegeneration marker linked to calcium binding adaptor molecule-1	TCCGAGGAGACG TTCAGCTA	CGTGTGACATC CACCTCCAA
S100B	cytosolic calcium-binding protein concentrated in astrocytes, is released following astroglia injury	GCGAATGTGACT TCCAGGAA	GCTTCCTAATT AGCTACAAC
BDNF (brain-derived neurotrophic factor)	Explains antioxidant and cholinergic transmission	CGGCGCCCATGA AAGAAGTA	TCGTTGGGCCG AACCTTCT

GFAP (glial fibrillary acidic protein)	Linkage with amyloid theory and its neuroinflammation	GTGCAGAGATGA TGGAGCTC	ACTGTTGGCCG TAAGCTGGT

5.3.7.5 Biochemical analysis

A thorough and intricate biochemical analysis was conducted on homogenized brain tissues harvested from mice, carefully adhering to the methodology outlined by Handa *et al.* [19].

Glutathione (GSH): To determine the levels of Glutathione within brain tissues, homogenate samples were combined with an equal volume of 5% sulfosalicylic acid. This mixture was then vigorously vortexed in an ice bath for a duration of 30 minutes, ensuring not only thorough mixing but also optimal cooling to preserve integrity of samples. After the mixing process, samples underwent centrifugation at 25000 rpm. This step was crucial for separating the supernatant, which was subsequently collected for further analytical procedures. The concentration of GSH was quantified using Ellman's reagent specifically the 5,5-dithiobis (2-nitrobenzoic acid) (DTNB) solution while absorbance readings were taken at a wavelength of 412 nm. The data obtained were expressed in micromoles of GSH per milligram of protein, calculated from a standard curve created from known concentrations of GSH, ensuring accuracy and reliability. Furthermore, the absorbance of solution was also recorded at 560 nm, using an advanced multimode plate reader, enabling precise and consistent measurements.

Malondialdehyde (MDA): To assess malondialdehyde levels, the TBARS (thiobarbituric acid reactive substances) method was employed. This meticulous examination commenced with rinsing the brain tissues three times using a chilled PBS solution, adjusted to a pH of 7.4. The tissues were then homogenized in PBS under the same pH conditions, incorporating 1 mM EDTA, all while maintaining low temperatures to safeguard the sample integrity. A 100 µL of the resulting supernatant was then mixed with sodium dodecyl sulphate (SDS) and incubated for a precise duration of 10 minutes. Following this incubation, 20% acetic acid was introduced to mixture, along with a 0.8% solution of thiobarbituric acid. To facilitate the necessary chemical reaction, reaction mixture was placed in a boiling water bath for 1 hour. The success of reaction was confirmed by emergence of a characteristic pink colour, which was then quantified through absorbance measurement at 532 nm. Standardization was achieved using 1,1,3,3-tetramethoxy propane (TMP), enabling the precise measurement of MDA levels, reported in millimoles per milligram of protein.

Reactive Oxygen Species (ROS): The quantification of ROS, specifically hydrogen peroxide (H_2O_2) and nitrite, was meticulously carried out within the brain tissues. An equal volume of Griess reagent was combined with supernatant and placed into a 96-well plate. This mixture was gently shaken during a 10-minute incubation in complete darkness to prevent any light-induced reactions. After this incubation period, the absorbance of resulting-coloured solution was measured at 540 nm. Known quantities of sodium nitrite were used to create a reliable standard curve, which facilitated the accurate quantification of brain homogenate samples under controlled conditions. The results of this analysis were expressed as micromoles per milligram of protein.

To measure ROS levels through the DCFDA approach, the fluorescent probe 2,7-Dichlorofluorescein diacetate was introduced into reaction. In this context, H_2O_2 served as a cellular peroxide, promoting conversion of DCFDA to its highly fluorescent form, DCF. A reaction mixture was carefully prepared with 10 mL of tissue homogenate sample, 5 µL of 5 µM DCFDA, and diluted with 985 µL of PBS at pH 7.4. A sophisticated multimode plate reader was used, calibrated to excitation and emission wavelengths of 485 nm and 525 nm, respectively. Fluorescence data were meticulously documented following a 30-minute incubation period, with the results reported in terms of fluorescence units per milligram of protein.

5.4. Results and discussion

5.4.1. Fabrication of Liposomes for Oxytocin and Vasopressin

Liposomes are one of the best advanced drug delivery systems that are used to deliver pharmaceutical drug(s) in multiple applications using various routes and therapy [26, 27].

Due to various advantages of liposome, it was decided to formulate liposomes of oxytocin and vasopressin for the management of neurological disorder.

5.4.2. Optimization of liposomes for oxytocin and vasopressin

5.4.2.1. Oxytocin loaded liposomes

Liposomes were prepared using different ratio of phospholipids in combination (Table 5.5). PS and PDI of various formulation (F1-F5) during lipid ratio optimization are tabulated in Table 5.5. HSPC was kept constant at 4 molar ratios while MPEG (2000)-DSPE: Cholesterol

was changed systemically. During the initial screening, lipid: polymer ratio of 4:0.5:0.5 was used and PS was found to be 146 nm with 0.342±0.06 PDI and 56.87% %EE respectively. Molar ratio of HSPC: MPEG (2000)-DSPE: Cholesterol (4:1:1) showed optimum results for PS, PDI & %EE. Further, stirring speed was optimised to find the maximum entrapment in liposomes. The speed of stirrer was varied from 100 to 400 rpm. The results showed that increasing stirring speed enhanced %EE of liposomes with controlled PS upto 300 rpm. However, with increasing stirring speed from 300 rpm to 400 rpm, the PS was reduced but drug entrapment was also reduced from 64% to 53 % (Table 5.6). Therefore, 300 rpm was finalised as optimum stirring speed for liposomal formulation. After stirring speed, time was also optimised. The stirring speed of 300 rpm was kept constant with time optimised for 30, 45 and 60 min (Table 5.7). With increasing stirring time, PS was reduced, but drug entrapment was decreased after 60 min. Therefore, 45 min stirring time was finalised.

Table 5.5: Optimization of ratio of lipids for oxytocin loaded liposomes formulation

Formulation code	HSPC: MPEG (2000)-DSPE: Cholesterol (molar)*	Particle size (nm)*	Polydispersity index (PI)*	Entrapment Efficiency (%)
F1	4:0.5:0.5	146.6±8.1	0.342±0.06	56.87±2.7
F2	4:1:0.5	108.6±7.2	0.251±0.09	58.34±2.6
F3	4:1.5:0.5	168.6±6.3	0.342±0.04	60.87±2.3
F4	4:1:1	95.06±0.86	0.115±0.002	64.03±0.54
F5	4:1:1.5	142.8±9.8	0.412±0.05	65.87±2.4
**n=6, data are represented as mean± SD*				

Table 5.6: Optimization with respect to stirring speed for oxytocin loaded liposomes formulation

Formulation code	stirring speed (RPM)*	Particle size (nm)*	Polydispersity index (PI)*	Entrapment efficiency (%)*
F6	100	189.2±16.23	0.75±0.09	51.1±2.2
F7	200	159.7±15.11	0.67±0.10	57.5±2.4
F8	300	95.06±0.86	0.115±0.002	64.03±0.54
F9	400	87.7±1.42	0.18±0.04	53.4±2.5
**n=6, data are represented as mean± SD*				

Table 5.7: Optimization of stirring time for oxytocin loaded liposomes formulation

Formulation code	Stirring time (min)*	Particle size (nm)*	Polydispersity index (PI)*	Entrapment efficiency (%)*
F_{10}	30	118.7±5.71	0.51±0.09	58.1±1.92
F_{11}	45	95.06±4.8	0.115±0.002	64.03±0.54
F_{12}	60	84.7±5.23	0.13±0.04	57.9±0.65
**n=6, data are represented as mean± SD*				

From the optimization studies outcome, the liposomes formulation (F11) was found to be the best and selected as final optimized formulation for further studies. The parameters used for preparation of this optimized formulation are recorded in below Table 5.8.

Table 5.8: Optimized parameters for oxytocin loaded liposomes formulation

Parameters	Optimized values
HSPC: MPEG (2000)-DSPE: Cholesterol (molar)	4:1:1 (w/w/w)
API	10mg/mL formulation
Stirring speed	300 RPM
Stirring time	45 min

5.4.2.2. Vasopressin loaded liposomes

Similarly, vasopressin loaded liposomes were also optimised. The parameters and results are tabulated from Table 5.9 to Table 5.12. During the initial screening, lipid: polymer ratio of 4:0.5:0.5 was used and PS was found to be 152.3±1.3 nm with 0.342±0.06 PDI. Though, % drug EE of liposomes varies with variation in lipid molar ratio from 57.23% to 66.76%, but molar ratio of PEG (2000)-DSPE: Cholesterol was 4:1:1 found to be optimum with good %EE, PS and PDI, as shown in Table 5.9. Further, stirring speed was optimised to find the maximum entrapment in liposomes. The results show that increasing stirring speed enhanced %EE of liposomes with controlled PS upto 300 rpm. However, with increasing stirring speed from 300 to 400 rpm, the PS was reduced but %EE was also reduced from 62.59±0.39 % to 46.1±1.9 % (Table 5.10). Therefore, 300 rpm was finalised as optimum stirring speed for liposomes formulation. After stirring speed, time was also optimised (Table 5.11). With increasing stirring time, PS was reduced but drug entrapment was decreased after 45 min stirring time. Therefore, 45 min stirring time was finalised.

5.4.3. Physicochemical attributes of optimised formulations

The average PS of oxytocin loaded liposomes (Oxy-Lipo) and Vasopressin loaded liposomes (Vas-Lipo) was found to be in the range from 50 nm to 100 nm with a unimodal distribution. Both the optimized Lipo had average PS of 95.06±0.86 nm for Oxy-Lipo & 99.06±1.01 nm for Vas-Lipo and PDI of 0.115±0.002 for Oxy-Lipo & 0.121±0.004 for Vas-Lipo (Table 5.13). For effective brain permeation, PS must be less than 200 nm, while formulation must exhibit PDI ≤0.150. The mean diameters of liposomes for the formulation were less than 100 nm as confirmed by TEM images of liposomes formulations of oxytocin and vasopressin (see Figure 5.2). The optimized Oxy-Lipo and Vas-Lipo formulation exhibited ZP of -22.1±0.12 mV and -21.8±0.17, respectively. The Lipo exhibited highest entrapment efficiency of 64.03±0.54 % for OXT-Lipo and 62.59±0.39 % for Vas-Lipo.

Table 5.9: Optimization with respect to ratio of lipids used cholesterol ratio for vasopressin loaded liposomes formulation

Formulation code	HSPC: MPEG (2000)-DSPE: Cholesterol (molar)	Particle size (nm)*	Polydispersity index (PI)*	Entrapment Efficiency (%)
F1	4:0.5:0.5	152.3±1.3	0.368±0.07	57.23±1.93
F2	4:1:0.5	113.1±6.4	0.581±0.06	68.26±1.76
F3	4:1.5:0.5	156.9±5.3	0.489±0.05	61.63±2.14
F4	4:1:1	99.06±1.01	0.121±0.004	62.59±0.39
F5	4:1:1.5	157.5±11.3	0.701±0.06	66.76±1.83
**n=6, data are represented as mean± SD*				

Table 5.10: Optimization with respect to stirring speed for vasopressin loaded liposomes formulation

Formulation code	Stirring speed (RPM)	Particle size (nm)*	Polydispersity index (PI)*	Entrapment efficiency (%)*
F6	100	178.20±17.1	0.690±0.08	50.20±1.9
F7	200	145.80±16.2	0.610±0.09	52.95±2.1
F8	300	99.06±1.01	0.121±0.004	62.59±0.39
F9	400	89.20±1.8	0.190±0.05	46.10±1.9
**n=6, data are represented as mean± SD*				

Table 5.11: Optimization of stirring time for vasopressin loaded liposomes formulation

Formulation code	Stirring time (min)	Particle size (nm)*	Polydispersity index (PI)*	Entrapment efficiency (%)*
F_{10}	30	145.9±6.21	0.51±0.09	59.20±2.12
F_{11}	45	99.06±1.01	0.121±0.004	62.59±0.39
F_{12}	60	79.7±1.13	0.13±0.04	55.20±0.75
**n=6, data are represented as mean± SD*				

From the optimization studies outcome, the liposomes formulation (F_{11}) was found to be best and selected as final optimized formulation for further studies. The parameters used for preparation of this optimized formulation are recorded in below Table 5.12.

Table 5.12: Optimized parameters for Liposomes for Vasopressin

Parameters	Optimized values
HSPC: MPEG (2000)-DSPE: Cholesterol	4:1:1 (*w/w/w*)
API	0.133 mg/mL formulation
Stirring speed	300 rpm
Stirring time	45 min

Table 5.13: Physicochemical attributes of optimised Oxytocin and Vasopressin loaded liposomes

Nano-formulation for	HSPC, MPEG (2000)-DSPE: Cholesterol	Particle size (nm)	PDI	Zeta Potential (mV)	%Drug Entrapment (EE)
Oxytocin	4:1:1	95.06±0.86	0.115±0.002	-22.1±0.12	64.03±0.54
Vasopressin	4:1:1	99.06±1.01	0.121±0.004	-21.8±0.17	62.59±0.39

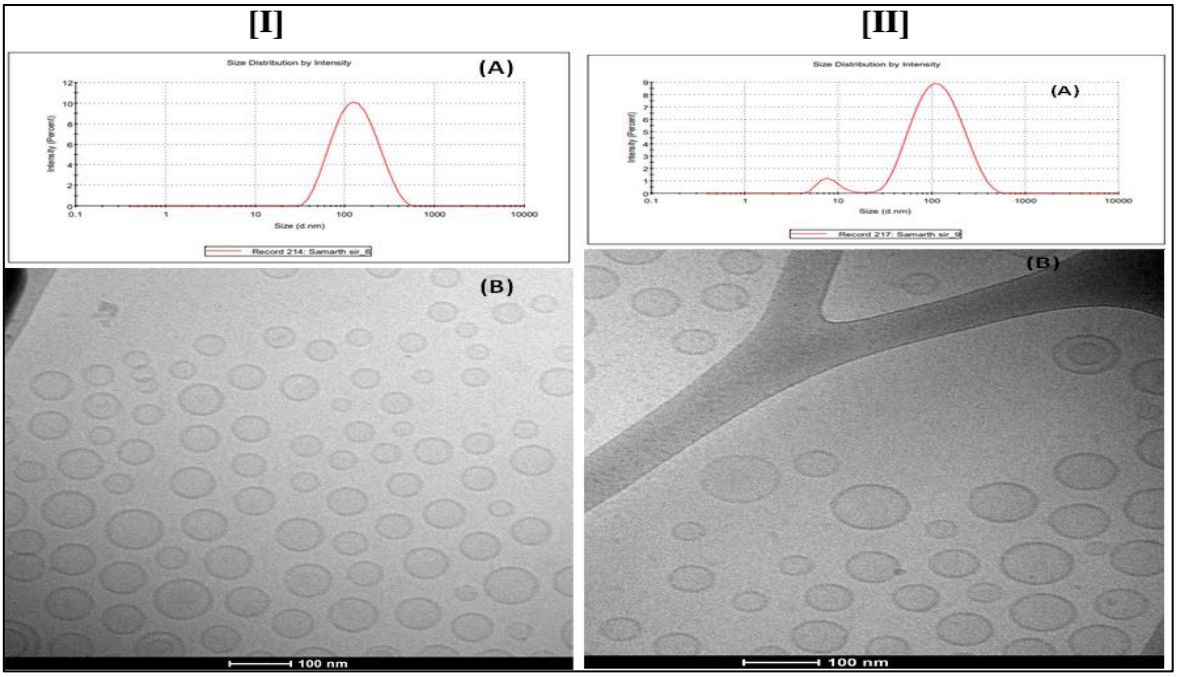

Figure 5.2: Graph of particle size analysis (A), and HR-TEM image (B) of oxytocin loaded liposomes and vasopressin loaded liposomes respectively.

5.4.4. Stability study of liposomes formulations

The stability of Oxytocin and Vasopressin- loaded Lipo dispersions were conducted at 2-8°C and 25±2°C/60±5%RH storage conditions. The stability data of CQAs PS, PDI, ZP and drug content of liposomes are tabulated in Table 5.14 & 5.15 for both drugs loaded Lipo.

5.4.4.1. Oxytocin-Loaded Liposomes

The ZP of liposomes initial to 6M during stability is from -22.1±0.12 to -23.4 ± 0.14 and -21.38 ± 0.24 at 5±3°C and 25±2°C/60±5%RH after 6M and 3M respectively. The observed, increasing PS from 99.06±1.01 nm to 112.5 ± 4.54 nm, 124.1 ± 4.54 nm, at 5±3°C and 25±2°C/60±5%RH after 6M and 3M respectively (Table 5.14). The PS increase at 25±2°C/60±5%RH is significantly more compared to 5±3°C after tested stability tenure. PS increase by increase in storage temperature is due to formation of multilaminar vesicles or aggregation. The PDI of Liposomes almost remains same at both storage conditions throughout the stability. The % of drug assay was decreased 99.32 ± 1.73 to 98.02 ± 1.12 at 5±3°C after 6M, while 97.21 ± 1.23 at 25±2°C/60±5%RH after 3M. Oxytocin in liposomes is more stable

at 5±3°C without loss of drug potency. Hence, we recommend 5±3°C storage condition to get maximum shelf life.

Table 5.14: Stability data of Oxytocin loaded liposomes

Storage condition	Time (M)	Zeta potential (mV)	Particle size (nm)	PDI	% Drug assay
Initial	0	-22.10±0.12	95.06±0.86	0.115±0.002	99.32 ± 1.73
5±3°C	1	-22.23±0.11	99.45±5.71	0.112±0.017	98.95 ± 1.91
	3	-20.70±0.17	101.34±4.34	0.111±0.007	98.45 ± 1.94
	6	-23.40±0.14	107.52 ± 6.21	0.107 ± 0.009	98.02 ± 1.12
25±2°C/60±5%RH	1	-24.38±0.15	111.32 ± 3.56	0.111 ± 0.045	98.19 ± 1.37
	2	-22.67±0.12	112.45 ± 3.97	0.110 ± 0.007	97.85 ± 1.82
	3	-21.38±0.24	115.76± 5.82	0.120 ± 0.005	97.21 ± 1.23

5.4.4.2. Vasopressin-Loaded Liposomes

The ZP of Liposome during stability was from -21.8±0.17 to -22.4 ± 0.84 and -24.8 ± 0.84 at 5±3°C and 25±2°C/60±5%RH after 6M and 3M respectively (Table 5.15). The observed, increasing PS from 99.06±1.01 to 112.5±4.54 nm & 124.1±4.54 nm at 5±3°C and 25±2°C/60±5%RH after 6M and 3M respectively. The PS increase at 25±2°C/60±5%RH was significantly more compared to 5±3°C after tested stability tenure. The increase of PS by increasing storage temperature was due to formation of multilaminar vesicles or aggregation. The PDI of Lipo almost remains same at both storage conditions throughout the stability. The % of drug assay was decreased from 98.02±1.87 to 96.89±1.25 at 5±3°C after 6M, while to 96.81±1.78 at 25±2°C/60±5%RH after 3M. As, Vasopressin in Lipo were more stable at 5±3°C without loss of drug potency. Therefore, it is 5±3°C storage condition is recommended to get maximum shelf life.

Table 5.15: Stability data of Liposomes for Vasopressin

Storage condition	Time (M)	Zeta potential (mV)	Particle size (nm)	PDI	% drug assay
Initial	0	-21.80 ± 0.17	99.06 ± 1.01	0.121 ± 0.004	98.02 ± 1.87
5±3°C	1	-20.03 ± 0.21	100.03 ± 4.21	0.125 ± 0.007	97.82 ± 1.57
	3	-22.70 ± 0.11	108.06 ± 1.01	0.126 ± 0.009	97.37 ± 1.34
	6	-22.40 ± 0.84	112.5 ± 4.54	0.118 ± 0.038	96.89 ± 1.25
25±2°C/60±5%RH	1	-22.38 ± 0.85	109.8 ± 5.48	0.25 ± 0.037	97.89 ± 2.76
	2	-23.67 ± 0.92	118.5 ± 6.67	0.34 ± 0.041	97.25 ± 1.67
	3	-24.80 ± 0.84	124.1 ± 4.54	0.38 ± 0.025	96.81 ± 1.78

5.4.5. *In vitro* cell line study

5.4.5.1. Evaluation on SH-SY5Y neuro cells

5.4.5.1.1 Cell viability and biocompatibility

The cell viability study was conducted on SH-SY5Y cells employing MTT assay to investigate biocompatibility of different formulations towards cells (Figure 5.3). Biocompatibility associated with Lipo formulation containing 1 µg/mL, 10 µg/ml and 100 µg/mL subsequent incubation with SH-SY5Y neuro cells for 24, 48 and 72 h was calculated (Figure 5.3). Although, it was observed that above 85% cell viability during increasing concentration at given time points (24 h, 48 h and 72 h) with Oxytocin, OXT-Lipo, Vasopressin and Vaso-Lipo. However, cell viability reduced from 95% to 85% after 72 h exposure of formulation at higher concentration (100 µg/mL). The cell viability above 85% at all tested conditions suggest that OXT and Vaso retained their biocompatibility on neuro-cells even after being loaded into liposomes. The encapsulation of drug into liposomes exhibited same neuro protective potential compared to that seen with plain OXT and Vaso. The probable reason for decreased cell viability at 72 h incubation is due to decreased cell proliferation in comparison to 24 and 48 h.

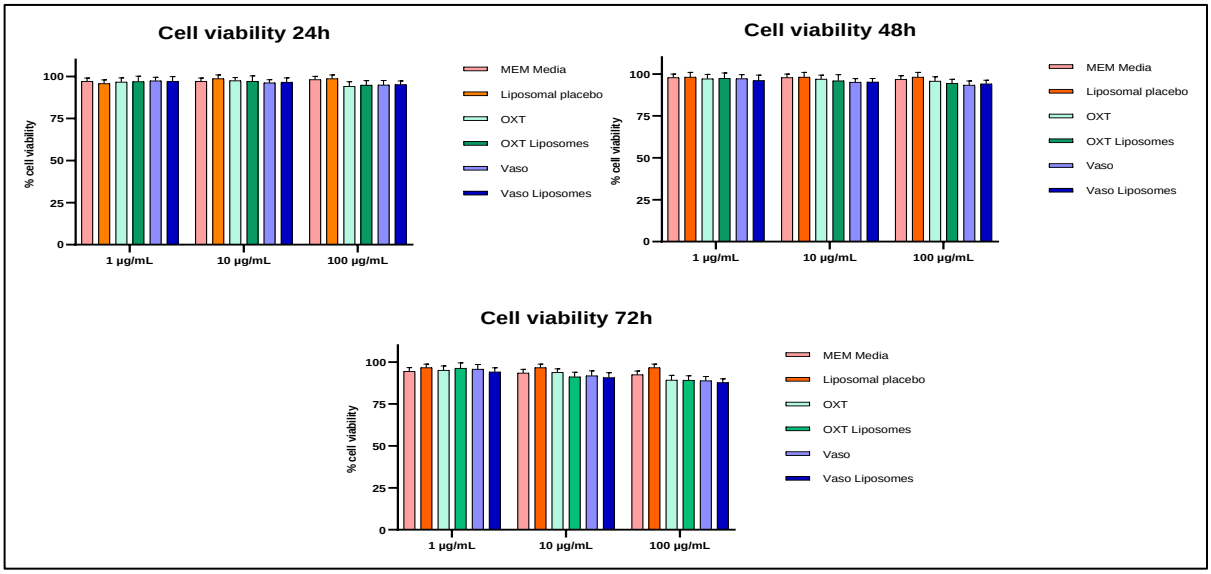

Figure 5.3: % Cell viability after the exposure of different formulations (plain and drug-loaded) after 24 h, 48 h & 72 h incubation.

5.4.5.1.2 Morphological observations

The influence of oxytocin, vasopressin, as well as Lipo loaded with these compounds, on the SH-SY5Y neuronal cells was investigated by closely analysing changes in cellular morphology. In this 100 µg/mL of concentration was studied for free drug and drug loaded liposomes (equivalent to drug). After a 48-hour exposure to both the pure drugs and the drug-loaded liposomes, no significant alterations in cellular structure were observed when viewed through a phase contrast microscope. In the SH-SY5Y cells treated with formulations, there were no visible signs of apoptosis, which typically include indicators such as disruption of cell membrane, reduction in cell size, and a decline in overall number of viable cells when compared to untreated control group. Figure 5.4 provides a visual comparison, showcasing the morphology of control cells alongside morphologies of treated cells.

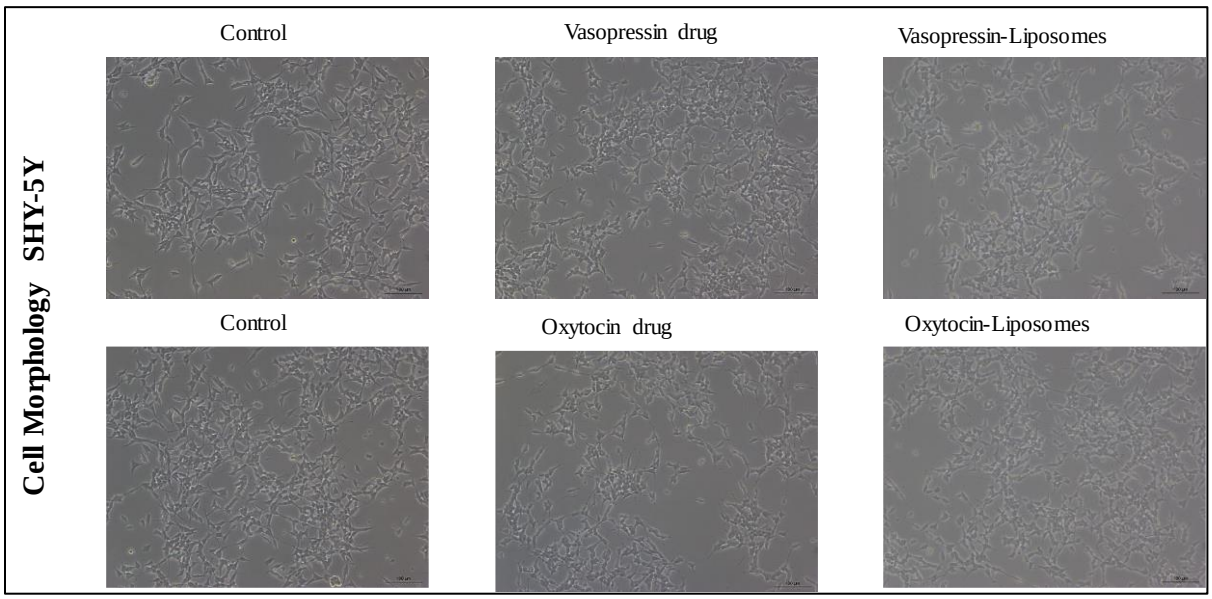

Figure 5.4: Morphological observation of SH-SY5Y cells treated with High dose (100 µg/mL) of vasopressin, oxytocin, vasopressin loaded liposomes and oxytocin loaded liposomes for 48 h at 20× magnification.

5.4.5.1.3 *In vitro* cell permeation study (Cell uptake*)*

A comprehensive study examining cell uptake of C6-OXT-Lipo, specifically C6-Vaso-Lipo, was conducted using SH-SY5Y cells to evaluate effectiveness with which these Lipo were internalized by cells. The results from this cell uptake evaluation revealed a strikingly higher internal localization of both OXT-Lipo and Vaso-Lipo following an incubation period of three

hours (Figures 5.5). These findings serve to support proposed hypothesis regarding cellular uptake of Liposomes, as indicated by persistent and vibrant fluorescence signals detected after 3 hours of incubation with the C-6 co-encapsulated Liposomes.

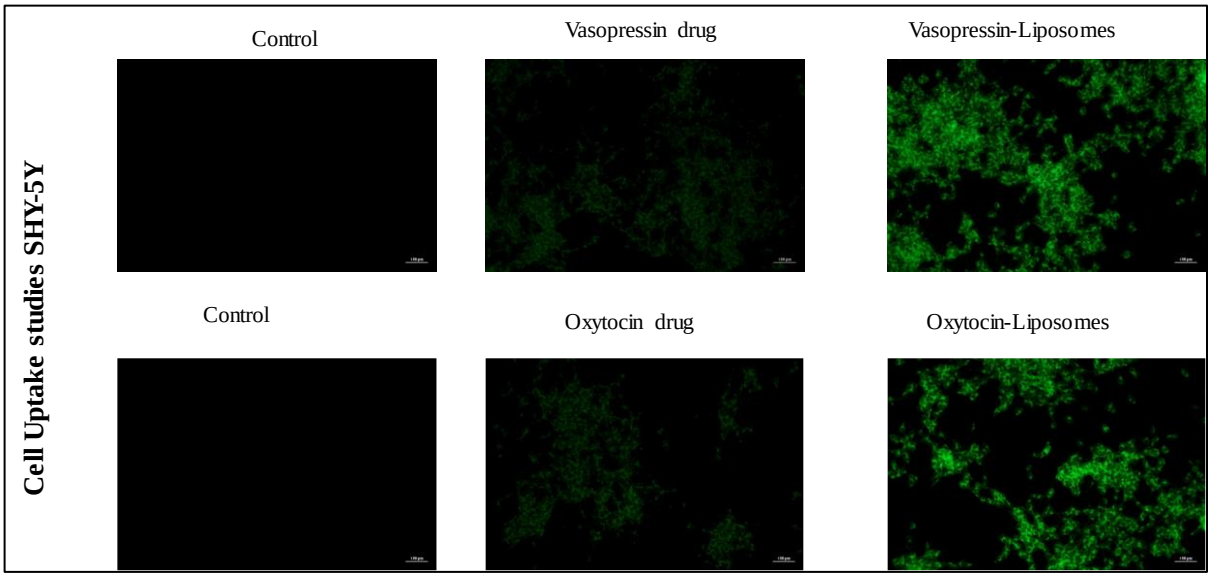

Figure 5.5: Cell uptake of SH-SY5Y cells treated with High dose (100 µg/mL) of vasopressin, oxytocin, vasopressin loaded liposomes and oxytocin loaded liposomes for 48 h at 20× magnification.

The notable increase in cellular uptake, attributed to substantial internalization of Lipo, strongly suggests that OXT and Vaso may experience an extended residence time within cellular environment. The OXT-loaded Lipo and Vaso-Lipo demonstrate a remarkable enhancement in processes of cellular uptake and permeation for both pharmaceutical compounds, indicating their potential as effective delivery systems.

Due to their lipid-based characteristics, these vesicles have a higher likelihood of reaching the cell surface while encountering significantly less steric hindrance, facilitating their entry into cells. These results imply a strong degree of biocompatibility and affinity between Lipo and SH-SY5Y cells, which ultimately leads to efficient internalization of vesicles by cells.

In addition, the cell uptake analysis provided vivid evidence of considerable cellular uptake of C-6-Lipo, showcasing the distribution of particles within cytoplasm, thereby effectively illustrating an enhanced internalization process. The cell uptake research corroborated that

these lipid-based nano-carriers are predominantly localized within cells rather than merely residing on cell surfaces. The observed improvement in uptake across cellular membranes can be intricately explained by several factors, including the nano-sized dimensions, distinctive shape, negative electrostatic charge, and inherent lipidic properties of the developed Lipo [12].

5.4.5.1.4 ROS (DCFDA) assay

A minimal level of ROS was detected following treatment with pure oxytocin, vasopressin, and their encapsulated Lipo. This was evidenced by the emission of green fluorescence, which resulted from the interaction between the produced ROS and the fluorescent dye DCF (Figure 5.6).

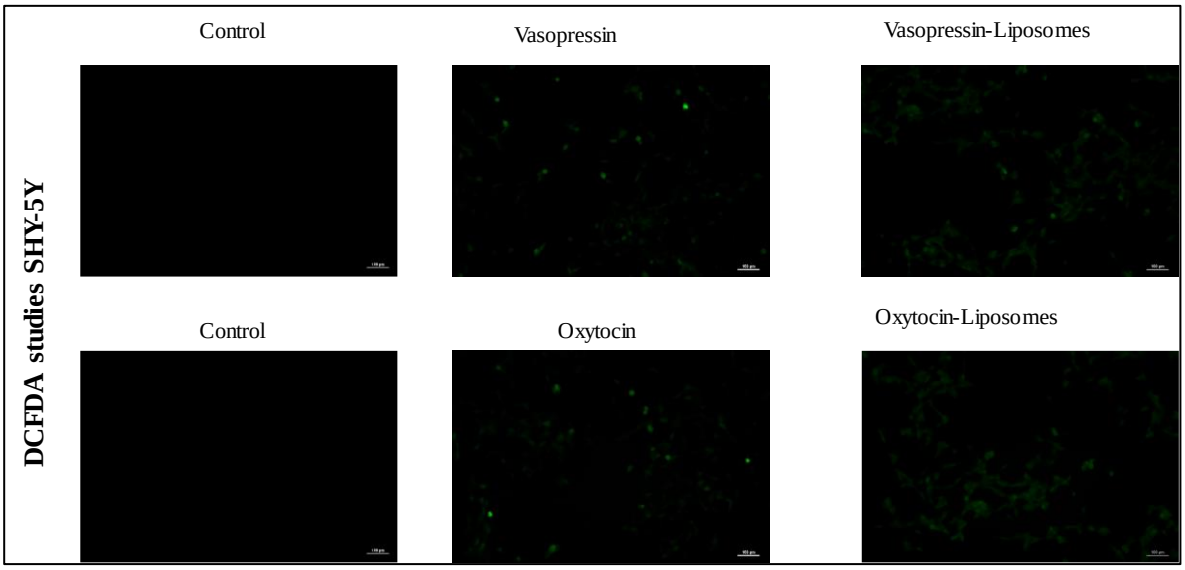

Figure 5.6: ROS generation of SH-SY5Y cells treated with control, Oxytocin, vasopressin, OXT-Liposomes and Vaso-liposomes at 100 µg/mL for 48 h at 20× magnification.

To quantify the results, the average intensity of ROS fluorescence from acquired images was meticulously analysed using Image J software. The analysis revealed that cells treated with both formulations exhibited ROS levels comparable to those of control group, as illustrated in Figure 5.6. These findings from ROS analysis imply that both OXT and Vaso sustained their biocompatibility in neuronal cells, even after being incorporated into Lipo. Furthermore, the encapsulation of these drugs into liposomes retained their neuroprotective potential, mirroring the effects observed with unaltered OXT and Vasopressin. The ROS analysis outcome suggest that OXT and vasopressin retained its biocompatible on neuro cells even after being

encapsulated within lipidic vesicles. The Oxytocin and vasopressin loaded vesicles depicted the similar neuro protective potential when compared with plain OXT and vasopressin. This implicates that, qualitatively OXT, vasopressin and their lipidic vesicles counterparts exhibit similar pattern or more precisely they all preserves neuro-protective nature equivalent to OXT and vasopressin.

5.4.5.1.5 Qualitative cell apoptosis assay (AO/EB staining)

Apoptosis was carefully evaluated in SH-SY5Y cells after exposure to pure oxytocin, vasopressin, oxytocin-loaded Lipo, and vasopressin-loaded Lipo by dual (AO/EB) staining techniques for visual assessment. In Figure 5.7, it is evident that the normal SH-SY5Y cells displayed intact nuclei, which were characterized by a moderate level of green fluorescence, indicating healthy cellular conditions.

In contrast, the treated SH-SY5Y cells, subjected to oxytocin, vasopressin, and their respective Lipo formulations, showed no discernible morphological changes typically associated with apoptosis. Key indicators such as nuclear condensation, increased brightness, and nuclear crinkling were absent, as confirmed by the AO/EB staining results. The control group cells maintained their viability, exhibiting a vibrant green fluorescence arranged in a circular pattern, with nuclei symmetrically centred, highlighting their overall health and structural integrity.

5.4.5.2 Evaluation on monocytic cells (THP-I)

5.4.5.2.1 Gene transcription analyses of inflammatory and apoptotic markers

The primary aim of study was to investigate impact of oxytocin, vasopressin, OXT-Lipo, and Vaso-Lipo on transcriptional profiles of various apoptotic and inflammatory immune markers. These markers included caspase-3, caspase-8, caspase-9, Akt1, NF-kβ, BCL-2, CD40, Bim, Bak, and IL-6, all of which play significant roles in cell death and inflammation [31].

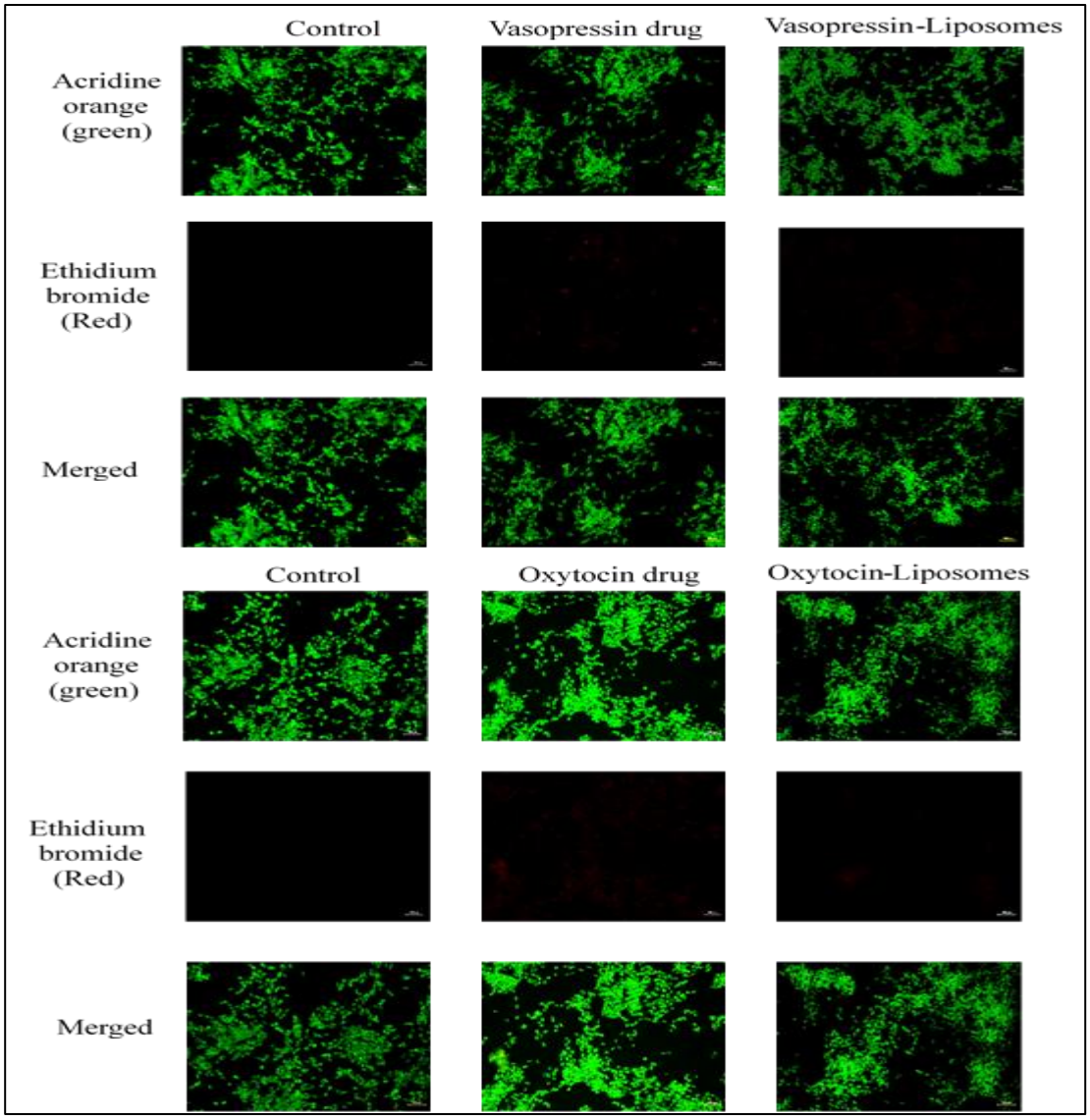

Figure 5.7: Acridine orange/Ethidium bromide dual staining studies of control, Vasopressin, vasopressin loaded liposomes, oxytocin and oxytocin loaded liposomes at high dose in SH-SY5Y cells for 48 h at 20× magnification.

There was a notable decrease in expression levels of pro-apoptotic markers' caspase-3 and caspase-8 in hTHP-I cells that were treated with all formulations of vasopressin and oxytocin (as depicted in Fig 5.8). In striking contrast, the expression of caspase-9 was elevated in treated group, indicating a complex interplay of signals. However, it is important to note that these variations in pro-apoptotic markers did not attain statistical significance. Moreover, a reduction in levels of inflammatory markers NF-kB and IL-6 was recorded in all treated cells exposed to

the various formulations of vasopressin and oxytocin. Cells that were treated with Lipo infused with vasopressin and oxytocin showed a significant reduction in BCL-2 expression, an important regulator of cell survival, in comparison to those that received standard drug treatment. Additionally, changes in expression of co-stimulatory markers were observed. The expression of CD40, implicated in regulating programmed cell death, along with pro-apoptotic gene Bak, was significantly reduced across all treated hTHP-I cells. Conversely, cells treated with oxytocin formulation exhibited an increase in expression levels of Bim, another pro-apoptotic marker.

The hTHP-I cells that received treatment with oxytocin displayed a highly significant reduction in expression of IL-6, a key pro-inflammatory cytokine, compared to both the cells treated with vasopressin and the untreated control group [31]. This suggests that oxytocin may play a vital role in modulating inflammatory responses in addition to its effects on apoptosis.

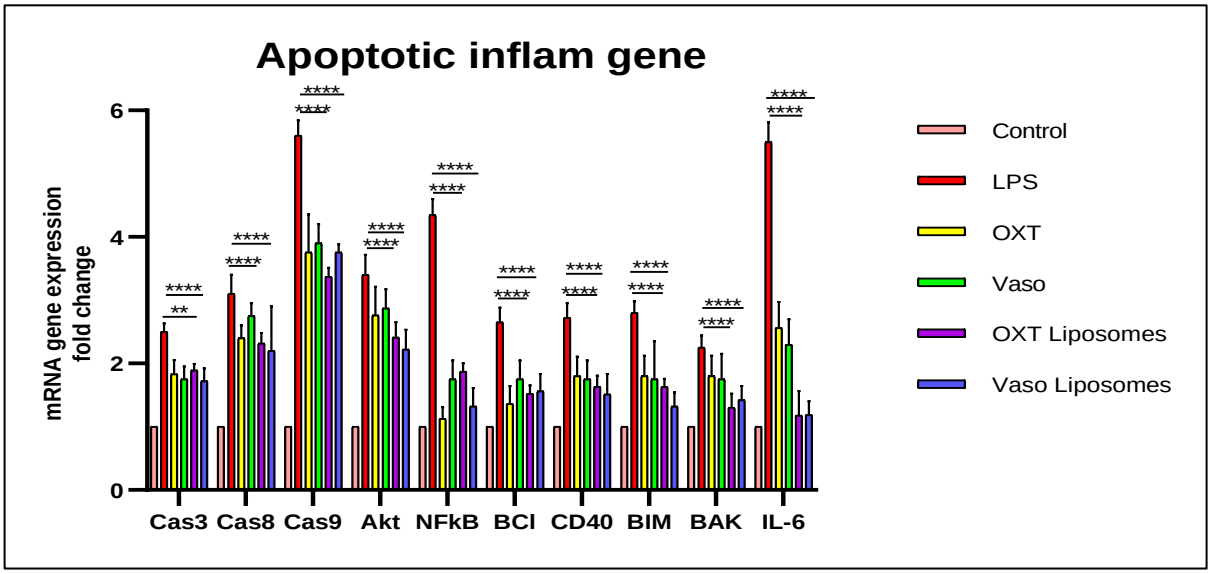

Figure 5.8: Determination of transcriptional gene expression of inflammatory, signalling and apoptotic markers

5.4.5.2.2. Confocal microscopy-based immunofluorescence assay (IFA)

The primary aim of this investigation was to establish a cell line model to enable us to explore the effects of various Lipo on the transcription factor FOXO1. This factor, in its phosphorylated state, is rendered inactive and plays a crucial role in regulating apoptotic pathways. Specifically, FOXO1 works in conjunction with the pro-apoptotic factor Bim, and their

regulation is tightly controlled by overexpression of co-stimulatory molecule CD40. This interaction mediates the signalling pathways of PI3-Akt within human THP-1 (hTHP-I) cells. The confocal microscopy assessed qualitative expression levels of FOXO1 in hTHP-I cells subjected to LPS stimulation. After 1 h post treatment with LPS, analysis revealed difference in FOXO1 expression when compared with LPS-stimulated cells to their unstimulated counterparts (as shown in Fig. 5.9).

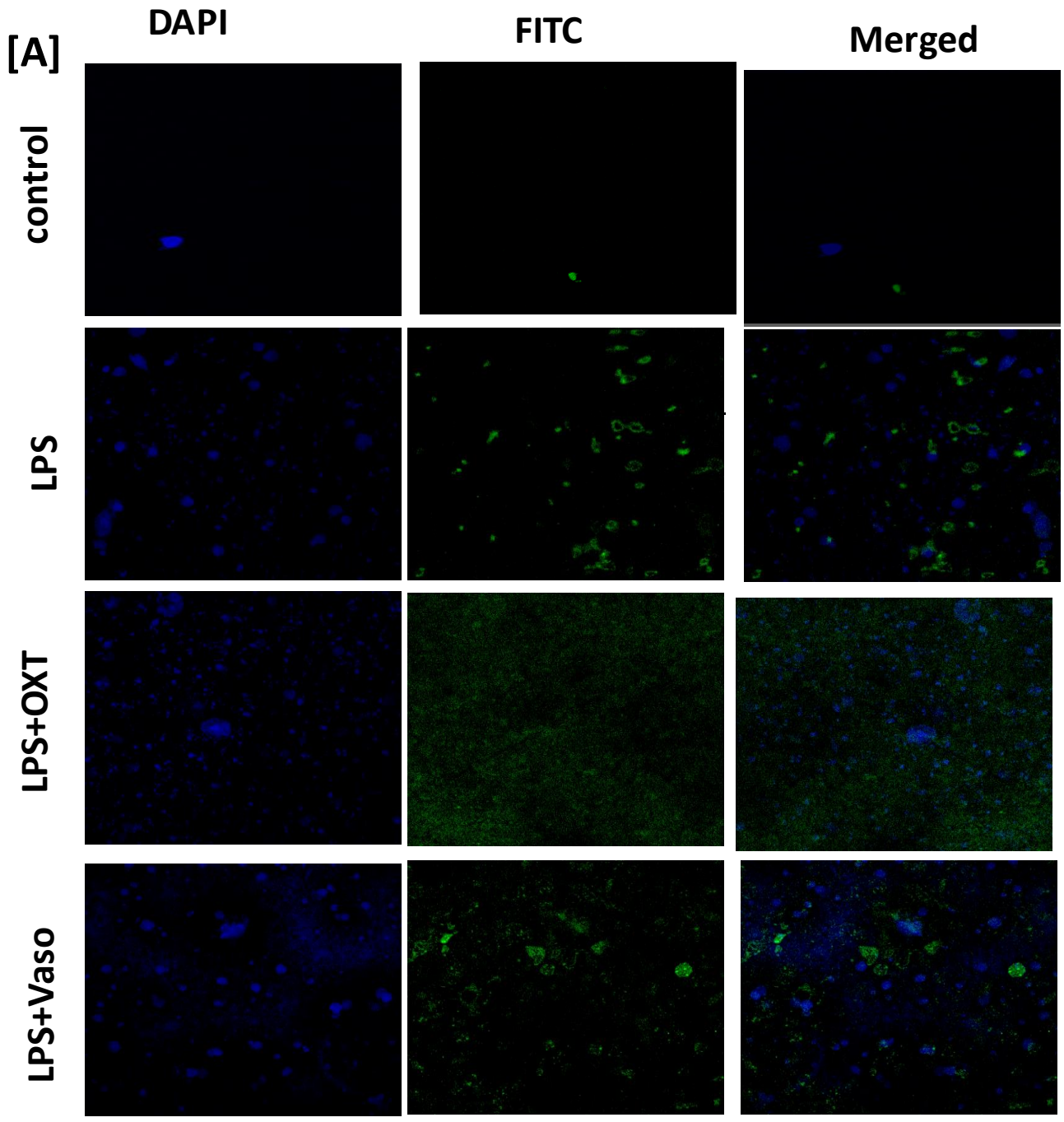
[A]
DAPI
FITC
Merged
control
LPS
LPS+OXT
LPS+Vaso

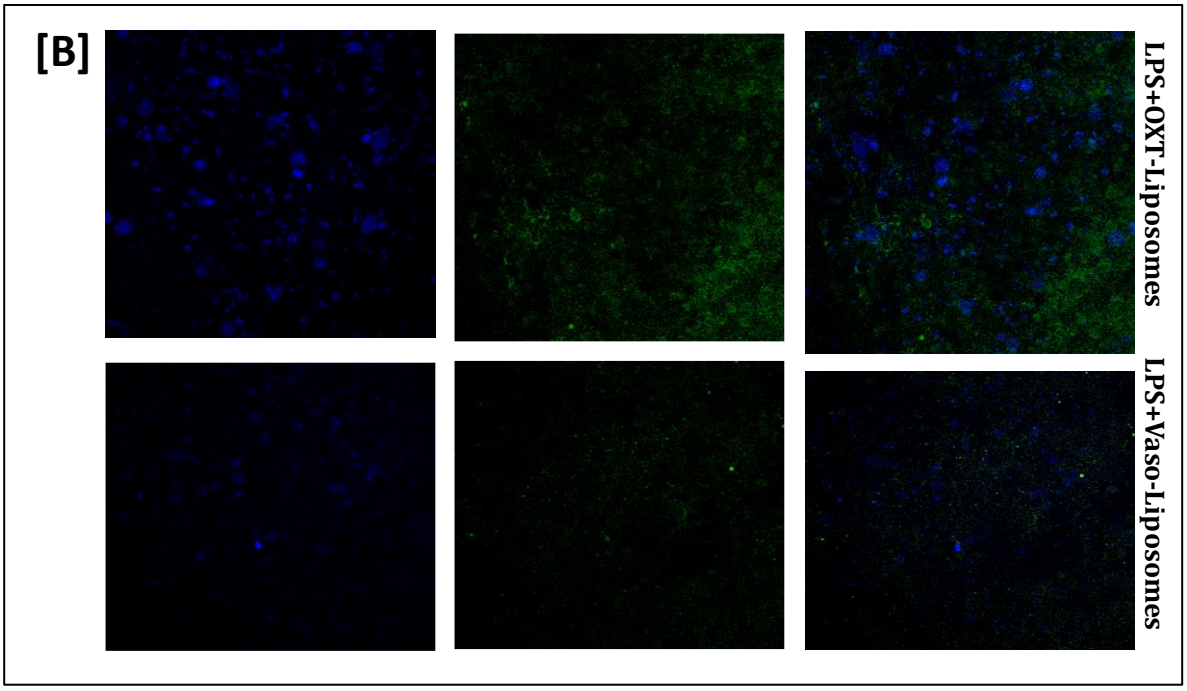

Figure 5.9 [A] & [B]: Expression of FOXO-1 gene following the LPS after various formulations treatment

5.4.5.3. Neurological effects of developed formulations in experimental animals

5.4.5.3.1. Oxytocin loaded Liposomes

5.4.5.3.1.1. Morris water maze test

The MWM test of oxytocin formulations was evaluated by comparing free oxytocin solution administered via IN & IV route vs oxytocin loaded Lipo administered *via* IN & IV route [16, 17, 26, 28]. The average mean time incurred for mice to reach on hidden platform was 37.16±6.75 seconds. Similarly, average mean time incurred for SCP mice to reach on hidden platform was 58.66±1.18 seconds i.e., 1.31 times more than placebo. Mice administered with Oxytocin *via* IN route were able to reach hidden platform in 39.58±4.45 seconds i.e., 1.07 and 0.67 times of placebo and SCP treated group (Figure 5.10). Similarly, mice administered with Oxytocin via IV route were able to reach hidden platform in 50.72±4.29 seconds i.e., 1.36 and 0.86 times of placebo and SCP treated group. However, mice administered with liposomal loaded oxytocin *via* IN route were able to reach hidden platform in 28.36±3.13 seconds i.e., 0.76 and 0.48 times of placebo and SCP treated group. Similarly, mice administered with liposomal loaded oxytocin via IV route were able to reach hidden platform in 44.45±4.23

seconds i.e., 1.20 and 0.76 times of placebo and SCP treated group. In this study, earlier the time to reach hidden platform more retention of memory by mice. The above cognitive based MWM study indicated Oxytocin when delivered via IN route whether in free form or loaded in liposomes effectively delivered Oxytocin to brain and reduced the time to reach hidden platform. Thus, it clearly implicated that IN route and liposomes effectively retained memory post treatment in comparison to naïve group.

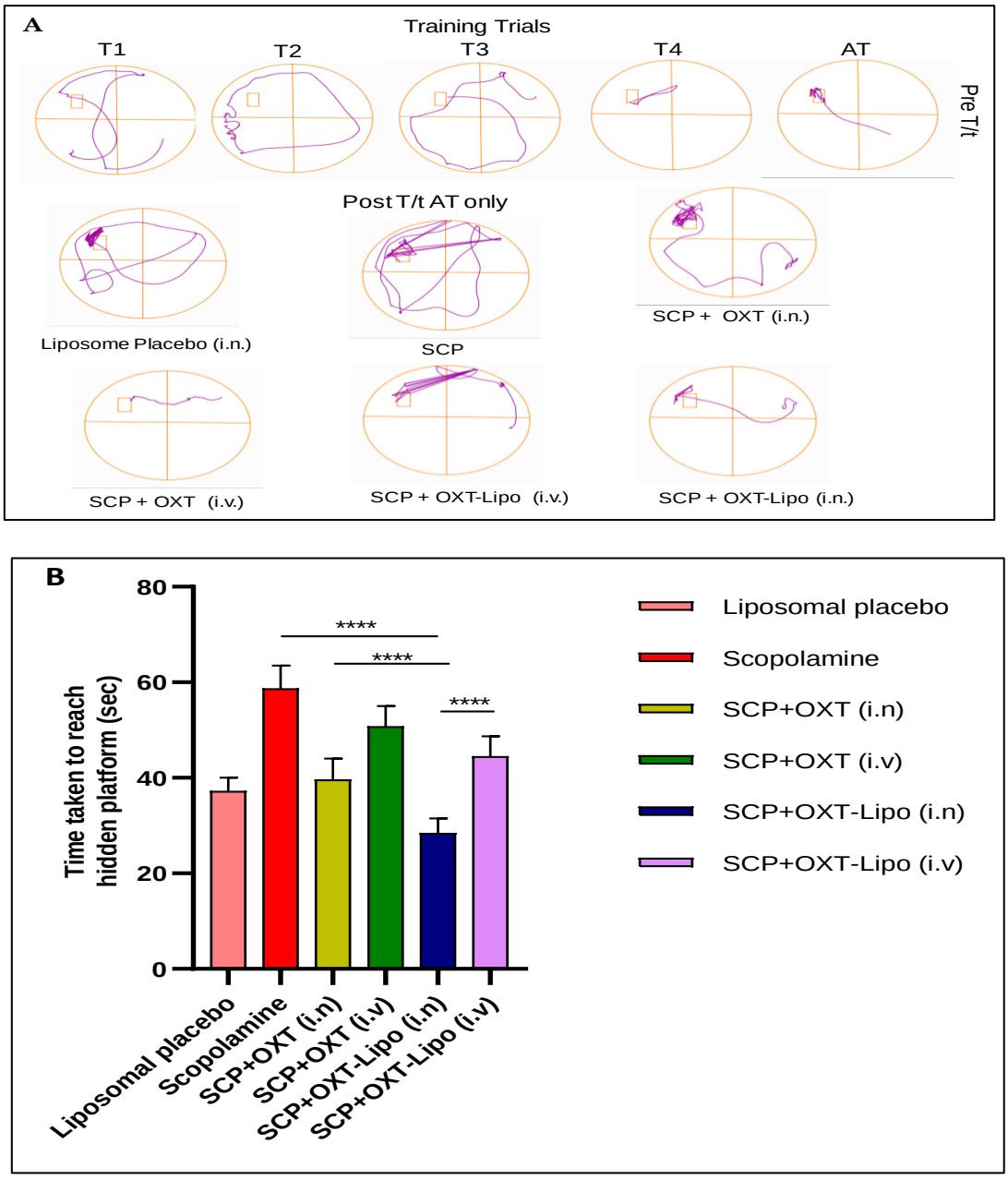

Figure 5.10: Pharmacological evaluation of formulations in Balb/C mice by Morris maze water studies. free oxytocin solution and oxytocin encapsulated liposomes administered via

i.n. & i.v. route. Data are represented for control (Ctrl), scopolamine treated (SCP), oxytocin loaded liposomes intranasal (IN) and intravenous (IV), oxytocin (IN) and oxytocin (IV). Figure A for acquisition trials, while figure B represents the time in seconds required by animal to reach the hidden platform.

5.4.5.3.1.2. Gene expression studies

To validate the molecular effectiveness of previously discussed treatment, comprehensive gene expression studies were conducted and found to be particularly important [18,19,28]. These studies involved an in-depth examination of brain homogenate samples, focusing on key biomarkers such as AIF-1, BDNF, and GFAP. Additionally, a thorough analysis pertaining to S100B was included in this investigation (Figure 5.11) [32].

The conducted neurobehavioral studies indicated that intranasal administration of Liposoaml-OXT demonstrates superior efficacy compared to traditional OXT delivery methods, including both intranasal and intravenous routes. To further substantiate these findings, gene expression profiling of brain homogenates from the respective treatment groups were performed. Specifically, the gene expression analysis was conducted on brains isolated from animals undergone to Morris Water Maze (MWM) test. The evaluation focused on the expression levels of AIF-1, S100B, BDNF, and GFAP in brain homogenate samples derived from both OXT and liposomal-OXT administered via Intranasal and Intravenous administration.

The quantitative PCR from brain sample extracted from treatment groups to establish effectiveness of the OXT, Liposomal-OXT administered via IN & IV route respectively. The transcription of following genes: AIF-1 (Allograft inflammatory factor 1), known for its role in inducing inflammation; BDNF (brain-derived neurotrophic factor), a critical protein involved in the survival and growth of neurons; GFAP (glial fibrillary acidic protein), a marker of astrocytic activation; IL-6 (interleukin-6), an important cytokine involved in inflammatory responses; and Nrf 2 (nuclear factor erythroid 2-related factor 2), a vital regulator of antioxidant response. These genes are pivotal to understand the underlying molecular mechanisms that may be crucial in conferring the therapeutic effects of the treatment. AIF-1 derives from the neutrophils, macrophages, and microglial cells, has been a well-known neurodegenerative marker associated with calcium binding adaptor molecule-1. The efficiency of Liposomal-OXT (IN) is marked by the expression of AIF-1. S100B is cytosolic calcium-

binding protein, present in astrocyte, and secreted during the astroglial injury. Therefore, S100B gene expression studies to detect neuronal damage/neurodegeneration due to overly expressed in neuroglial cells. Eventually, these expression studies clearly suggested the prominent neutralization effect of intranasally administered Liposomal-OXT. As GFAP is directly associated with the neuroinflammation, the brain tissue relative mRNA expression was seen similar to that with the untouched control. However, a many fold reduction in GFAP expression in the experimental (scopolamine treatment) AD was seen in group treated with intranasal Liposomal-OXT. Whereas the intravenously administered OXT reduced the GFAP expression but not to the extent as with the intranasal formulation.

The higher relative expression of BDNF, GFAP and S100b in Liposomal-OXT and OXT given intranasally and intravenously treated group. A remarkable elevation in the expression of these markers was seen in the control (without AD) group. Whereas the experimental induced AD mice receiving intranasal treatment with the Liposomal-OXT showed the increased expression of BDNF to that with the untouched control. Whereas BDNF expression was seen lower with other formulation and route of administration. More precisely, BDNF expression usually lower in AD patients in comparison to normal patients. Since the BDNF expression indicates the antioxidant and cholinergic transmission. Similar, pattern was observed in case of BDNF expression of intranasal Liposomal-OXT and naïve mice brains. This means that intranasal Liposomal-OXT is able to regulate BDNF expression in similar pattern to naive group. The pattern of BDNF expression was in order of SCP < OXT (IV) < Lipo-OXT (IV) < OXT (IN) < Lipo-OXT (IN) < Naïve group. The lower BDNF expression simulates to literature report of AD patients and higher BDNF expression simulates to literature report of normal patients. BDNF expression of intranasal Liposomal-OXT group also simulates to naïve group that clearly indicates the efficiency of route and liposomal system.

Increased GFAP levels were correlated with increased amyloid β levels and declined cognition. This GFAP is present in astrocytes. GFAP primarily marks its elevated expression both in serum and CSF of AD patients. The similar fashion was observed in our studies also. GFAP levels were in order of SCP > OXT (IV) > Lipo-OXT (IV) > OXT (IN) > Lipo-OXT (IN) > Naïve group. The decreased expression in CSF of intranasal Liposomal-OXT group and naïve group clearly indicates that IN route and intranasal Liposomal-OXT showed efficacy and similarity in pattern to naïve group.

S100b is a neuroprotective factor i.e., governed by neuroinflammation and its expression tends to upregulate in AD patients and it is expressed lower in normal patients. Similar pattern was observed in current research. The levels of S100b was found to be in order of SCP > OXT (IV) > Lipo-OXT (IV) > OXT (IN) > Lipo-OXT (IN) > Naïve group. This order clearly signifies the efficacy of intranasal Liposomal-OXT when administered via IN route.

AIF expression was correlated with neuronal cell death in cortex and hippocampal area of brain. The AIF expression was seen reduced with conjugated OXT administered intranasally similar to control. AIF expression was in order of SCP > OXT (IV) > Lipo-OXT (IV) > OXT (IN) > Lipo-OXT (IN) > Naïve group. This is probably due to the protective sheath for OXT due to liposomal to protect OXT from physiological attacks of nasal environment and administration via IN route that clearly defines the efficacy of route and liposome from above studies.

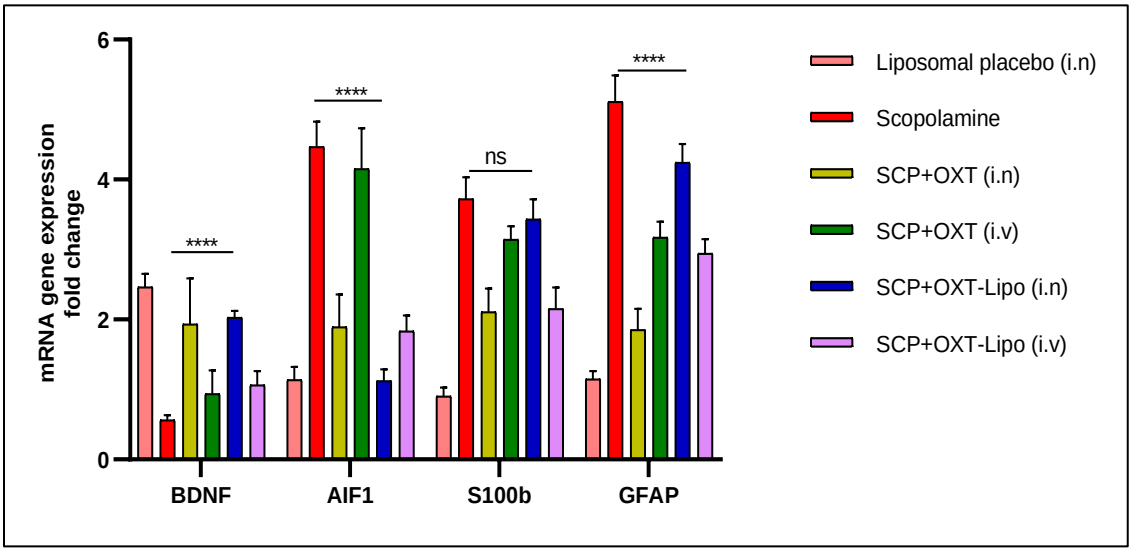

Figure 5.11: Gene expression of brain with different treatment groups. Data are represented for control (Ctrl), scopolamine treated (SCP), oxytocin loaded liposomes intranasal (IN) and intravenous (IV), oxytocin (IN) and oxytocin (IV)

In conclusion of the current study, gene expression levels show clearly the impact of routes of administration. The neuro protective effect of oxytocin in brain can be increased by intranasal route and further by encapsulation into lipidic liposomes for nose to brain delivery.

5.4.5.3.1.3. Biochemical estimations

The biochemical assessment of brain homogenate samples was conducted on animals treated with various forms of oxytocin, including free oxytocin administered IV and IN, as well as oxytocin encapsulated in lipid carriers through both routes. This evaluation aimed to explore the effects of these treatments in comparison to a positive control group (naïve) and a negative control group that received SCP treatment (Figure 5.12).

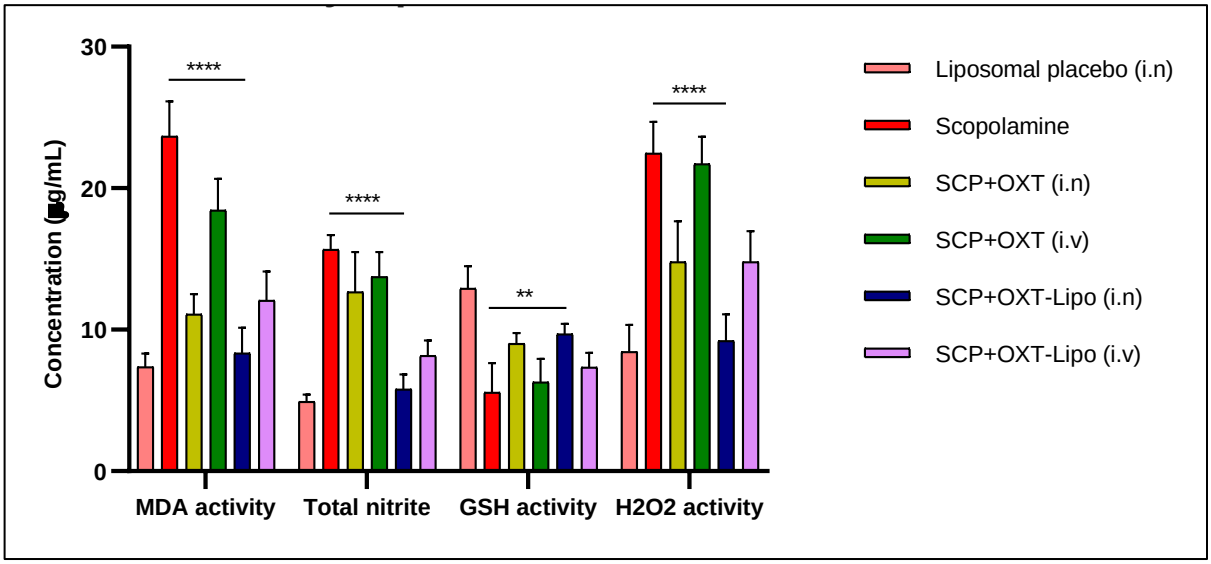

Figure 5.12: Biochemical estimation of brain homogenates with different treatment groups. Data are represented for control (Ctrl), scopolamine treated (SCP), oxytocin loaded liposomes intranasal (IN) and intravenous (IV), oxytocin (IN) and oxytocin (IV)

MDA levels tends to rise in AD patients due to formation of peroxidation in brain and serum samples. MDA expression directly influences the oxidative stress in AD. Similarly, nitrite activity seems to be in similar fashion in AD patients as nitric oxide is one of the by-products. GSH expression is inversely proportion to oxidative stress. More GSH means patient is less prone to AD and lower the GSH patient is more prone to AD. H_2O_2 degrading activity is directly proportional to ROS. More the presence of H_2O_2 signifies the presence of oxidative stress due to inability of physiological system of brain to degrade it. And more accumulation leads to neuronal damage and neuroinflammation.

The prepared brain homogenate from naiv̈e, mice with experimental mice (by the SCP treatment), mice receiving free OXT & liposomal OXT through both intravenous and intranasal routes were studied.

The SCP treatment showed higher secretion of MDA (lipid peroxidation biomarker), nitrite and peroxide activity levels and significantly comparative to naïve control group. However, OXT & Liposomal-OXT administered via IV route also showed the higher MDA, nitrite and peroxide activity levels in comparison to OXT & Liposomal-OXT administered via IN route. Intranasal Liposomal-OXT reduced the MDA, nitrite and peroxide activity levels similar to naïve control. Summarizing, levels of MDA, nitrite and peroxide activity were in order of: SCP > OXT (IV) > Lipo-OXT (IV) > OXT (IN) > Lipo-OXT (IN) > Naïve group.

The reduced levels in treated group signifies that, OXT administered in liposomal and as such via IN route is more effective to deduce AD related biochemical parameters. Apart from that intranasal Liposomal OXT tends to be present in therapeutic concentrations in brain when compared to with OXT & liposomal OXT administered via IV route.

The antioxidant GSH levels were in order of: SCP < OXT (IV) < Lipo-OXT (IV) < OXT (IN) < Lipo-OXT (IN) < Naïve group. The higher level in intranasal Liposomal OXT signifies that more OXT is able to reach in brain and tends to sustain in biological environment of brain in therapeutic levels. Apart from that, plain & Liposomal OXT injected through intravenous route showed the protective effect by controlling GSH activity but not in significance to intranasal Liposomal-OXT group.

The above cognitive, gene expression and biochemical studies revealed about intranasal Liposomal OXT dominance in terms of efficacy over the plain OXT when delivered via IN route in SCP mice. This clearly establishes that OXT when administered in form of liposome tends to sustain in brain for longer intervals when compared with plain and effectively delivered molecule at site of choice.

5.4.5.3.1.4. Brain Histopathology examinations

The comparative difference in effectiveness of formulation suggested in current study is indicated by histological evaluation of hippocampal observations. Higher the neuronal density, more promising the treatment [28]. The density of neurons was found to be higher in naïve

group followed by oxytocin loaded liposomal formulation delivered via IN route, oxytocin delivered via IN route, oxytocin delivered via IV route, oxytocin loaded liposomal formulation delivered via IV route and SCP treated group (Figure 5.13). The neuronal density is main functionality of human brain where it is directly proportional to effectiveness of treatment. So, in this study, higher neuronal density was observed in group where no treatment was provided, followed by group treated with Oxytocin Loaded in liposomes delivered via IN route.

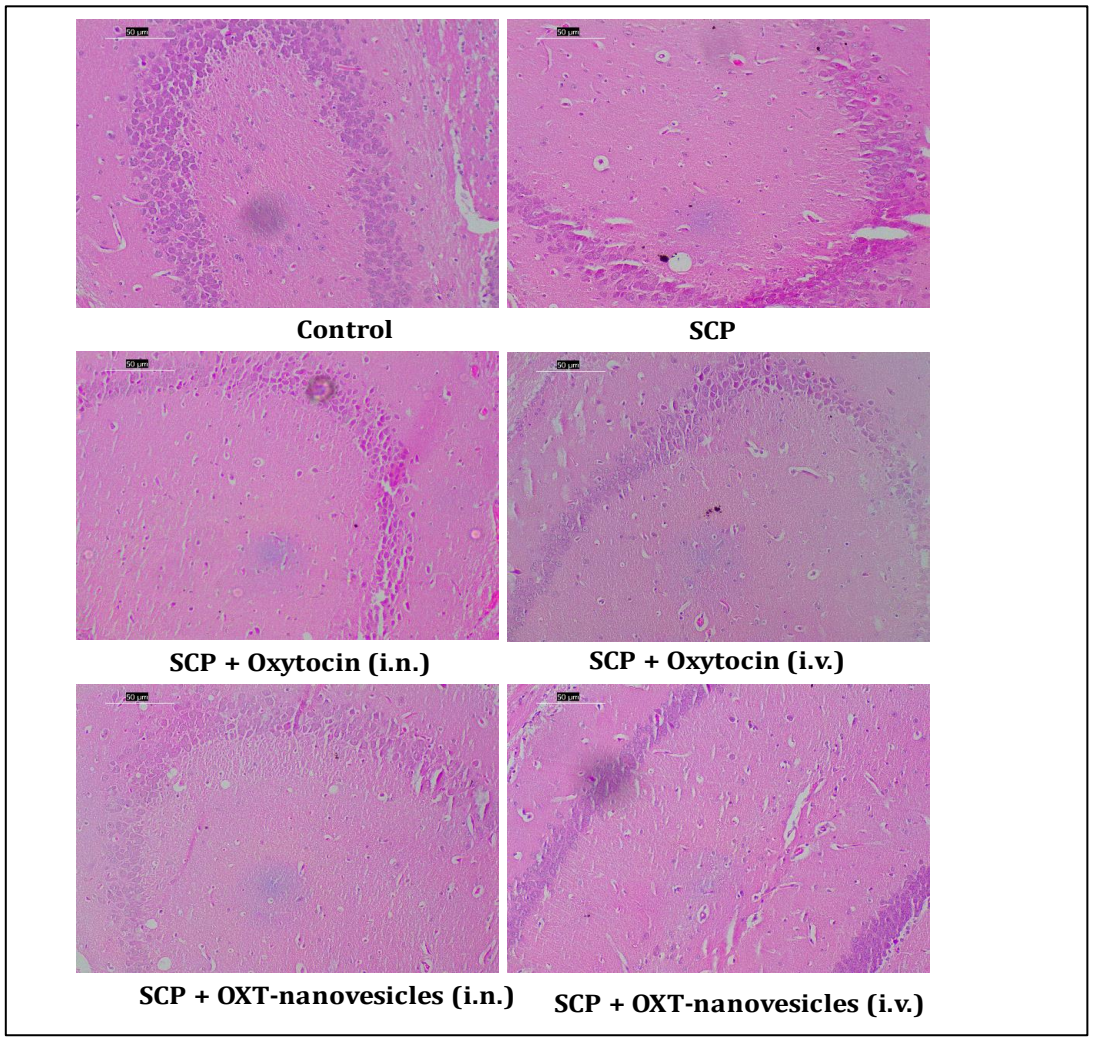

Figure 5.13: Images of histopathology evaluation of brain Hippocampus of Balb/C with scale 50 μm. Animals treated with free oxytocin solution and oxytocin encapsulated liposomes administered via i.n. & i.v. route. Data are represented for control (liposomes placebo), scopolamine treated (SCP), oxytocin loaded liposomes intranasal (i.n) and intravenous (i.v.), oxytocin (i.n.) and oxytocin (i.v.)

5.4.5.3.2. Vasopressin loaded Liposomes

Scopolamine is a competitive, nonselective blocker of muscarinic receptors. The cholinergic hypothesis on aging and AD served as the foundation for the scopolamine model and was a key factor in its development.

5.4.5.3.2.1. MWM test

The MWM test was done to compare free vasopressin solution administered *via* IN & IV in comparison to vasopressin loaded liposomes administered *via* IN & IV route [19].

The comparative results are presented in Figure 5.14. The average mean time incurred for mice to reach on hidden platform was 37.16±6.75 seconds. Similarly, average mean time incurred for SCP mice to reach on hidden platform was 58.66±1.18 seconds. Mice administered with Vasopressin via IN route were able to reach hidden platform in 40.05±4.87 seconds i.e., 1.08 and 0.68 times of placebo and SCP treated group. Similarly, mice administered with Vasopressin via IV route were able to reach hidden platform in 48.42±5.58 seconds i.e., 1.3 and 0.83 times of placebo and SCP treated group.

However, mice administered with liposomal loaded vasopressin *via* IN route were able to reach hidden platform in 30.87±3.37 seconds i.e., 0.83 times and 0.53 times of Placebo and SCP treated animals. Similarly, mice administered with liposomal loaded vasopressin via IV route were able to reach hidden platform in 36±2.54 seconds. In this study, earlier the time to reach hidden platform more retention of memory by mice. The above cognitive based MWM study indicated that Vasopressin when delivered via IN route whether in free form or loaded in liposomes could effectively deliver Vasopressin to brain and reduce the time to reach hidden platform. Thus, it clearly implicated that IN route and liposomes effectively retained memory post treatment in comparison to naïve group.

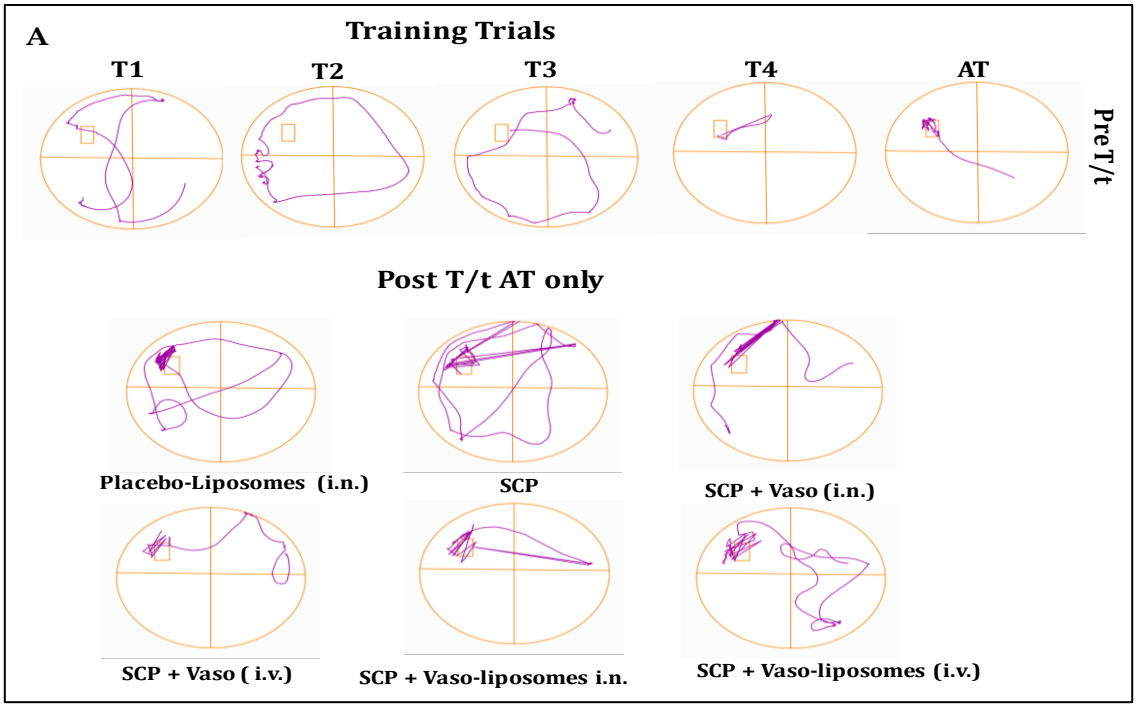

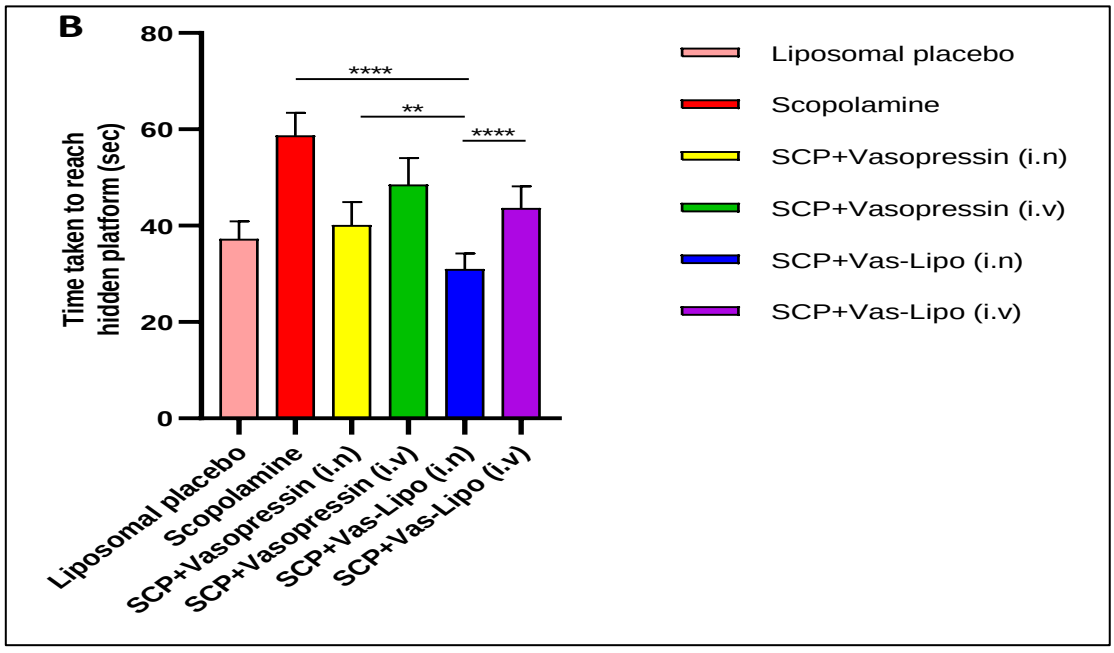

Figure 5.14: Pharmacological evaluation of formulations in Balb/C mice by Morris maze water studies. free vasopressin solution and vasopressin encapsulated liposomes administered via i.n. & i.v. route. Data are represented for control (Ctrl), scopolamine treated (SCP), vasopressin loaded liposomes intranasal (i.n) and intravenous (i.v.), vasopressin (i.n.) and vasopressin (i.v.). Figure A for acquisition trials, while figure B represents the time spent by animal to reach the hidden platform

5.4.5.3.2.2. Gene expression

Gene expression studies were performed as in Section 5.4.5.3.1.2. The pictorial data (Figure 5.15) clearly visualizes effect of treatment on various gene expression studies. The expression of BDNF follows pattern as: SCP < Vaso (IV) < Lipo-Vaso (IV) < Vaso (IN) < Lipo-Vaso (IN) < Naïve group. AIF expression studies were observed as follows: SCP > Vaso (IV) > Lipo-Vaso (IV) > Vaso (IN) > Lipo-Vaso (IN) > Naïve group. GFAP expression was found to be: SCP > Vaso (IV) > Lipo-Vaso (IV) > Vaso (IN) > Lipo-Vaso (IN) > Naïve group. S100b expression was found to be: SCP > Vaso (IV) > Lipo-Vaso (IV) > Vaso (IN) > Lipo-Vaso (IN) > Naïve group. In conclusion of the current study, gene expression levels are clearly impacted by the route of administration. The neuro protective effect of vasopressin in brain can be increased by intranasal route and further by encapsulation into lipidic liposomes for nose to brain delivery.

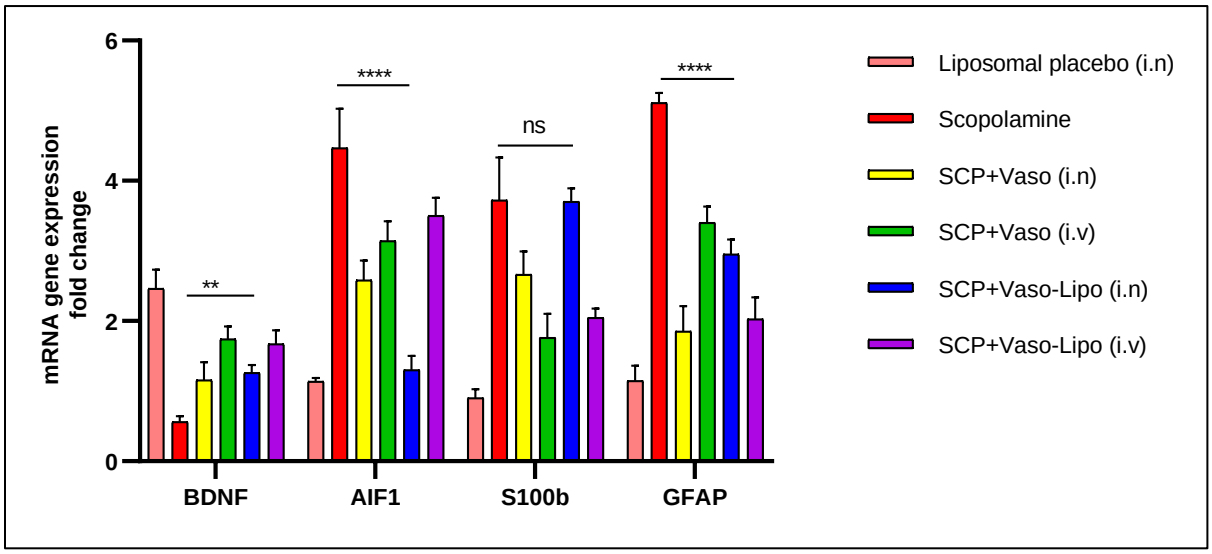

Figure 5.15: Gene expression level of brain samples. Data are represented for control (Ctrl), scopolamine treated (SCP), vasopressin loaded liposomes intranasal (i.n) and intravenous (i.v.), vasopressin (i.n.) and vasopressin (i.v.).

5.4.5.3.2.3. Biochemical estimations

The brain homogenate biochemical studies were done for naiv̈e, SCP-treated, free Vasopressin solution (IV & IN) and Vasopressin loaded lipidic carriers (IV & IN).

The levels of naïve groups were found to be significantly higher than those of the SCP-treated group. When compared to another group, the treatment group's antioxidant level was the greatest in GSH experiments (Figure 5.16).

SCP tends to decrease GSH content (antioxidant) and increase MDA levels. In SCP presence, stress levels such as nitrite and H_2O_2 also rise in tandem with an increase in MDA levels. As a result, the biochemical estimation revealed that the formulation's MDA, nitrite, and H_2O_2 levels had significantly decreased. The order for MDA, nitrite, and H_2O_2 levels was as follows: SCP > Vaso (IV) > Lipo-Vaso (IV) > Vaso (IN) > Lipo-Vaso (IN) > Naïve group. It was found that in naïve group levels of each of these parameters were remarkable higher than the SCP-treated group. According to GSH studies, the treatment group showed the highest antioxidant level when compared to another group. The order for GSH was SCP < Vaso (IV) < Lipo-Vaso (IV) < Vaso (IN) < Lipo-Vaso (IN) < Naïve group.

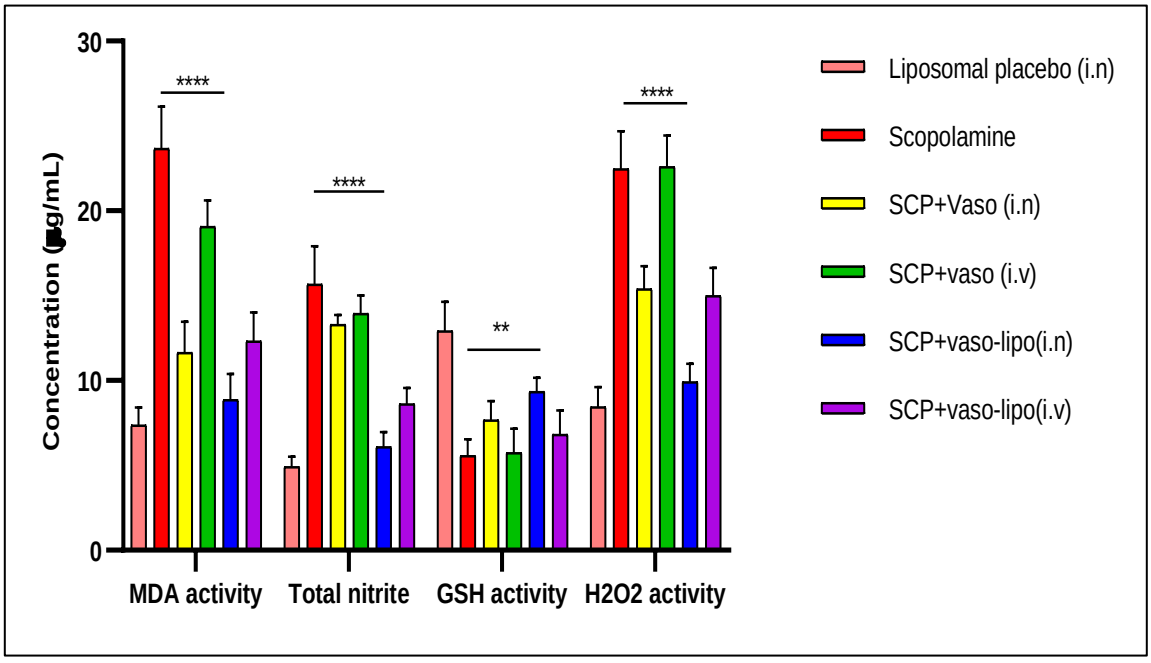

Figure 5.16: Biochemical estimation of brain homogenates. Data are represented for control (Ctrl), scopolamine treated (SCP), vasopressin loaded liposomes intranasal (i.n) and intravenous (i.v.), vasopressin (i.n.) and vasopressin (i.v.).

5.4.5.3.2.4. Brain histopathology examinations

The histological assessment of hippocampal observations indicates the relative differences in the effectiveness of Lipo suggested in current study. Higher neuron density shows more efficacious treatment of formulations [28]. The density of neurons was found to be higher in naïve group followed by vasopressin loaded liposomal formulation delivered via Intranasal route, vasopressin delivered via Intranasal route, vasopressin delivered via Intravenous route, vasopressin loaded liposomal formulation delivered via Intravenous route, and SCP treated group (Figure 5.17). The neuronal density is main functionality of human brain where it is directly proportional to effectiveness of treatment. So, in this study higher neuronal density was observed in group where no treatment was provided, followed by group treated with vasopressin loaded in liposomes delivered via IN route.

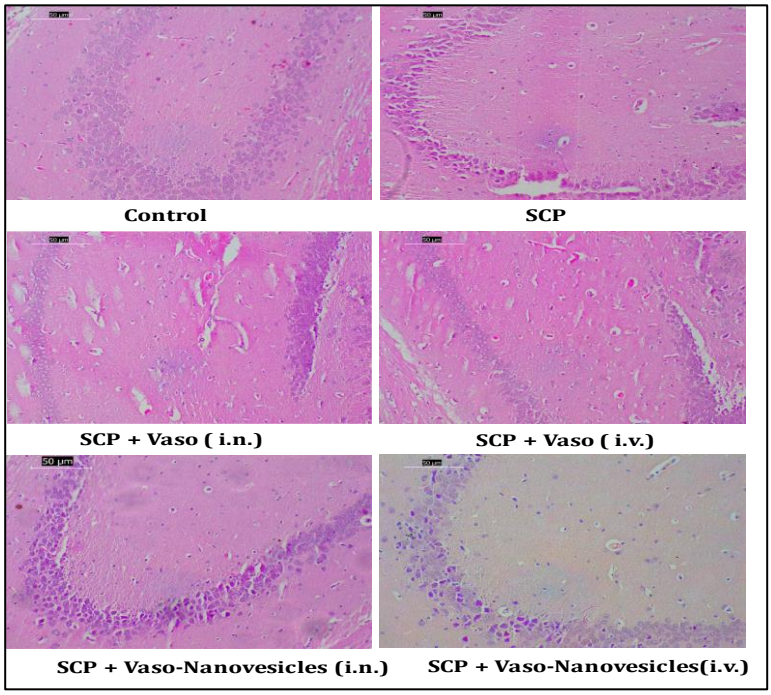

Figure 5.17: Images of histopathology evaluation of brain Hippocampus of Balb/C with scale 50 µm. Animals treated with free vasopressin solution and vasopressin encapsulated liposomes administered via i.n. & i.v. route. Data are represented for control (Naïve), scopolamine treated (SCP), SCP+vasopressin loaded liposomes intranasal (i.n) and intravenous (i.v.), SCP+ vasopressin (i.n.), and SCP+ Vasopressin (i.v.).scopolamine treated (SCP), SCP+vasopressin loaded liposomes intranasal (i.n) and intravenous (i.v.), SCP+ vasopressin (i.n.), and SCP+ Vasopressin (i.v.).

References

1 Upadhyay RK. Drug delivery systems, CNS protection, and the blood brain barrier. BioMed research international. 2014;2014(1):869269.

2 Handa M, Singh A, Bisht D, Kesharwani P, Shukla R. Potential of particle size less than 15 nm via olfactory region for direct brain delivery via intranasal route. Health Sciences Review. 2022 Sep 1;4:100038.

3 Pardridge WM. Drug transport across the blood–brain barrier. Journal of cerebral blood flow & metabolism. 2012 Nov;32(11):1959-72.

4 Trevino JT, Quispe RC, Khan F, Novak V. Non-invasive strategies for nose-to-brain drug delivery. Journal of clinical trials. 2020;10(7).

5 Clayton KN, Salameh JW, Wereley ST, Kinzer-Ursem TL. Physical characterization of nanoparticle size and surface modification using particle scattering diffusometry. Biomicrofluidics. 2016 Sep 1;10(5).

6 Rodriguez-Loya J, Lerma M, Gardea-Torresdey JL. Dynamic light scattering and its application to control nanoparticle aggregation in colloidal systems: a review. Micromachines. 2023 Dec 22;15(1):24.

7 Jain A, Agarwal A, Majumder S, Lariya N, Khaya A, Agrawal H, Majumdar S, Agrawal GP. Mannosylated solid lipid nanoparticles as vectors for site-specific delivery of an anti-cancer drug. Journal of Controlled Release. 2010 Dec 20;148(3):359-67.

8 Negi P, Aggarwal M, Sharma G, Rathore C, Sharma G, Singh B, Katare OP. Niosome-based hydrogel of resveratrol for topical applications: An effective therapy for pain related disorder (s). Biomedicine & Pharmacotherapy. 2017 Apr 1;88:480-7.

9 Garg NK, Singh B, Sharma G, Kushwah V, Tyagi RK, Jain S, Katare OP*. Development and characterization of single step self-assembled lipid polymer hybrid nanoparticles for effective delivery of Methotrexate. RSC Advances 2015;5 (77): 62989-62999.

10 Lopez-Suarez L, Al Awabdh S, Coumoul X, Chauvet C. The SH-SY5Y human neuroblastoma cell line, a relevant in vitro cell model for investigating neurotoxicology in human: Focus on organic pollutants. Neurotoxicology. 2022 Sep 1;92:131-55.

11 Dravid A, Raos B, Svirskis D, O'Carroll SJ. Optimised techniques for high-throughput screening of differentiated SH-SY5Y cells and application for neurite outgrowth assays. Scientific reports. 2021 Dec 14;11(1):23935.

12 Garg NK, Singh B, Kushwah V, Sharma R, Tyagi RK, Jain S, Katare OP*. The ligand (s) anchored lipobrid nanoconstruct mediated delivery of methotrexate: an effective approach in breast cancer therapeutics. *Nanomedicine: Nanotechnology, Biology, and Medicine* 2016; 12: 2043–2060.

13 Dong QM, Ling C, Zhao L. Immunofluorescence analysis of cytokeratin 8/18 staining is a sensitive assay for the detection of cell apoptosis. Oncology letters. 2015 Mar 1;9(3):1227-30.

14 Barth M, Toto Nienguesso A, Navarrete Santos A, Schmidt C. Quantitative proteomics and in-cell cross-linking reveal cellular reorganisation during early neuronal differentiation of SH-SY5Y cells. Communications Biology. 2022 Jun 7;5(1):551.

15. Singhai AK, Jain S, Jain NK. Evaluation of an aqueous injection of ketoprofen. Pharmazie 1997, 52, 2149–2151

16. Kesharwani P, Tekade RK and Jain NK. Formulation development and in vitro–in vivo assessment of the fourth-generation PPI dendrimer as a cancer-targeting vector. Nanomedicine. 2014, 9(15), pp.2291-2308.

17 Maher R, Moreno-Borrallo A, Jindal D, Mai BT, Ruiz-Hernandez E, Harkin A. Intranasal polymeric and lipid-based nanocarriers for CNS drug delivery. Pharmaceutics. 2023 Mar;15(3):746.

18 Handa M, Sanap SN, Bhatta RB, Patil GP, Ghose S, Singh DP, Shukla R, Rahul Shukla Combining donepezil and memantine via mannosylated PLGA nanoparticles for intranasal delivery: Characterization and preclinical studies, Biomaterials Advances, 2023, 154, 213663

19 Handa M, Sanap SN, Bhatta RB, Patil GP, Ghose S, Singh DP, Shukla R, Rahul Shukla. Simultaneous Intranasal Codelivery of Donepezil and Memantine in a Nanocolloidal Carrier: Optimization, Pharmacokinetics, and Pharmacodynamics Studies. Molecular PharmaceuticsVol 20/Issue 9

20 Livak KJ, Schmittgen TD, Analysis of Relative Gene Expression Data Using Real-Time Quantitative PCR and the 2−ΔΔCT Method. Methods Volume 25, Issue 4, December 2001, Pages 402-408

21 Maher R, Moreno-Borrallo A, Jindal D, Mai BT, Ruiz-Hernandez E, Harkin A. Intranasal polymeric and lipid-based nanocarriers for CNS drug delivery. Pharmaceutics. 2023 Mar;15(3):746.

22 Dighe S, Jog S, Momin M, Sawarkar S, Omri A. Intranasal Drug Delivery by Nanotechnology: Advances in and Challenges for Alzheimer's Disease Management. Pharmaceutics. 2023 Dec 29;16(1):58.

23 Vorhees CV, Williams MT. Morris water maze: procedures for assessing spatial and related forms of learning and memory. Nature protocols. 2006 Aug;1(2):848-58.

24 Yang ZF, Ho DW, Lau CK, Lam CT, Lum CT, Poon RT, Fan ST. Allograft inflammatory factor-1 (AIF-1) is crucial for the survival and pro-inflammatory activity of macrophages. International immunology. 2005 Nov 1;17(11):1391-7.

25 De Leon-Oliva D, Garcia-Montero C, Fraile-Martinez O, Boaru DL, García-Puente L, Rios-Parra A, Garrido-Gil MJ, Casanova-Martín C, García-Honduvilla N, Bujan J, Guijarro LG. AIF1: function and connection with inflammatory diseases. Biology. 2023 May 9;12(5):694.

26 Marianecci C, Carafa M. Smart nanovesicles for drug targeting and delivery. Pharmaceutics. 2019 Mar 29;11(4):147.

27 Mondal J, Pillarisetti S, Junnuthula V, Surwase SS, Hwang SR, Park IK, Lee YK. Extracellular vesicles and exosome-like nanovesicles as pioneering oral drug delivery systems. Frontiers in Bioengineering and Biotechnology. 2024 Jan 8; 11:1307878.

28 Mehta M, Bui TA, Yang X, Aksoy Y, Goldys EM, Deng W. Lipid-based nanoparticles for drug/gene delivery: An overview of the production techniques and difficulties encountered in their industrial development. ACS Materials Au. 2023 Aug 21;3(6):600-19.

29 Yang ZF, Ho DW, Lau CK, Lam CT, Lum CT, Poon RT, Fan ST. Allograft inflammatory factor-1 (AIF-1) is crucial for the survival and pro-inflammatory activity of macrophages. International immunology. 2005 Nov 1;17(11):1391-7.

30 Vorhees CV, Williams MT. Morris water maze: procedures for assessing spatial and related forms of learning and memory. Nature protocols. 2006 Aug;1(2):848-58.

31 Sharma P, Tandel N, Kumar R, Negi S, Sharma P, Devi S, Saxena K, Chaudhary NR, Saini S, Kumar R, Chandel BS, Sijwali PS, Tyagi RK. Oleuropein activates autophagy to circumvent anti-plasmodial defense. iScience 27, 109463, April 19, 2024

32 De Leon-Oliva D, Garcia-Montero C, Fraile-Martinez O, Boaru DL, García-Puente L, Rios-Parra A, Garrido-Gil MJ, Casanova-Martín C, García-Honduvilla N, Bujan J, Guijarro LG. AIF1: function and connection with inflammatory diseases. Biology. 2023 May 9;12(5):694

33 Garg NK, Tyagi RK, Sharma G, Jain A, Singh B, Jain S, Katare OP*. Functionalized Lipid-Polymer Hybrid Nanoparticles Mediated Codelivery of Methotrexate and Aceclofenac: A Synergistic Effect in Breast Cancer with Improved Pharmacokinetics Attributes. *Molecular Pharmaceutics* 2017:14(6):1883-1897

34 Garg NK, Singh B, Jain A, Sharma R, Nirbhavane P, Tyagi RK, Kushwah V, Jain S, Katare OP. Fucose decorated solid-lipid nanocarriers mediate efficient delivery of methotrexate in breast cancer therapeutics. *Colloids and Surfaces B: Biointerfaces* 2016; 146: 114–126